What drives the latitudinal gradient in open ocean surface dissolved inorganic carbon concentration?

Yingxu Wu[1], Mathis P. Hain[1], Matthew P. Humphreys[1,2], Sue Hartman[3], Toby Tyrrell[1]

[1]University of Southampton, National Oceanography Centre Southampton, Southampton, UK
5 [2]Centre for Ocean and Atmospheric Sciences, School of Environmental Sciences, University of East Anglia, Norwich, UK
[3]National Oceanography Centre, Southampton, UK

Correspondence to: Yingxu Wu (Yingxu.wu@soton.ac.uk)

Abstract. Previous work has not led to a clear understanding of the causes of spatial pattern in global surface ocean DIC,
10 which generally increases polewards. Here, we revisit this question by investigating the drivers of observed latitudinal gradients in surface salinity-normalized DIC (nDIC) using the Global Ocean Data Analysis Project Version 2 (GLODAPv2) database. We used the database to test three different hypotheses for the driver producing the observed increase in surface nDIC from low to high latitudes. These are: (1) sea surface temperature, through its effect on the CO_2 system equilibrium constants, (2) salinity-related total alkalinity (TA), and (3) high latitude upwelling of DIC- and TA-rich deep waters. We find
15 that temperature and upwelling are the two major drivers. TA effects generally oppose the observed gradient, except where higher values are introduced in upwelled waters. Temperature-driven effects explains the majority of the surface nDIC latitudinal gradient (182 out of 223 µmol kg^{-1} in the high-latitude Southern Ocean). Upwelling, which has not previously been considered as a major driver, additionally drives a substantial latitudinal gradient. Its immediate impact, prior to any induced air-sea CO_2 exchange, is to raise Southern Ocean nDIC by 220 µmol kg^{-1} above the average low latitude value. However, this
20 immediate effect is transitory. The long-term impact of upwelling (brought about by increasing TA), which would persist even if gas exchange were to return the surface ocean to the same CO_2 as without upwelling, is to increase nDIC by 74 µmol kg^{-1} above the low latitude average.

1 Introduction

The ocean absorbs about one quarter of the anthropogenic CO_2 emitted every year (Le Quéré et al., 2018). It is the largest non-
25 geological carbon reservoir (~38000 Gt C) (Falkowski et al., 2000), containing 50 times as much carbon as the pre-industrial atmosphere, and thereby plays an important role in modulating the Earth's climate system. Approximately 97% of the oceanic carbon pool exists in the form of dissolved inorganic carbon (DIC) (Falkowski et al., 2000), which is defined as the sum of the concentrations of aqueous CO_2, bicarbonate and carbonate ions:

$$DIC = [CO_2^*] + [HCO_3^-] + [CO_3^{2-}] \tag{1}$$

where $[CO_2^*]$ refers to the sum of aqueous CO_2 and true carbonic acid (H_2CO_3), with the latter negligible (Zeebe and Wolf-Gladrow, 2001).

Understanding the distribution of DIC in seawater is essential for understanding anthropogenic CO_2 invasion (Gruber, 1998; Humphreys et al., 2016; Lee et al., 2003; Sabine et al., 1999; Sabine et al., 2002; Vázquez-Rodríguez et al., 2009) and ocean acidification (Doney et al., 2009; Orr et al., 2005). Given that the surface ocean is where most organisms live, and that it is the part of the ocean that exchanges CO_2 with the atmosphere, the controls on surface DIC particularly merit investigation.

Many previous studies focused on the vertical rather than the horizontal distribution of DIC, aiming to understand the relative contributions of the different "carbon pumps" in controlling DIC variations throughout the water column (i.e., solubility pump, soft tissue pump, and carbonate pump, see details in Cameron et al., 2005; Gruber and Sarmiento, 2002; Toggweiler et al., 2003a; Toggweiler et al., 2003b). However, the solubility pump is so named because it is based on an assumption about the horizontal distribution of surface DIC – that DIC is high where new deep waters form at high latitudes, because of the effect of temperature on CO_2 solubility.

Previous work on the horizontal distribution of surface DIC included development of an algorithm to approximately reproduce the global surface DIC distribution (Lee et al., 2000), in which salinity-normalized DIC (nDIC) was predicted from empirically-derived functions of sea surface temperature and nitrate that varied seasonally and geographically. Key et al. (2004) depicted the global distribution of surface DIC based on an earlier version (GLODAPv1) of the dataset used here, noting that the surface DIC pattern is overall more similar to nutrients (including in the Southern Ocean, where both DIC and nutrients are enriched) than to salinity, unlike total alkalinity (TA) whose pattern more closely resembles that of salinity (Fry et al., 2015). Using the data from the new GLODAPv2 database (Key et al., 2015; Olsen et al., 2016), surface DIC is confirmed here to have its highest values at high latitudes, like nutrients, and to reach its lowest values in the equatorial zone in each basin (Fig. 1a; more details in Sect. 3.1). Earlier studies (Lee et al., 2000; Toggweiler et al., 2003a; Williams and Follows, 2011, Sect. 6.3 "What controls DIC in the surface ocean?") suggested that temperature is of primary importance in regulating surface DIC; under this assumption, surface waters in cool regions at high latitudes should hold more DIC than surface waters in the warm regions at low latitudes (Williams and Follows, 2011, Toggweiler et al., 2003a). Temperature may also drive latitudinal differences in carbonate ion concentration and surface aragonite saturation state (Ω_{arag}) (Jiang et al., 2015; Orr et al., 2005), through its effect on CO_2 solubility and CO_2 system thermodynamics.

Unlike previous studies, Williams and Follows (2011) argued that another variable also exerts a secondary control on the surface DIC distribution: at a given DIC, TA influences the seawater partial pressure of carbon dioxide (see also Omta et al., 2011), and therefore air-sea gas exchange. Takahashi et al. (2014) subsequently explored the seasonal climatological distributions of surface DIC using seawater pCO$_2$ from the Lamont Doherty Earth Observatory (LDEO) database and TA estimated from sea surface salinity, qualitatively attributing seasonal differences (on a regional scale) to the greater upward mixing of high-CO_2 deep waters in winter and summer biological carbon drawdown. Their study pointed out the great potential of upwelling to alter surface DIC, but it was focused more on controls on DIC seasonality rather than DIC spatial variability.

In recent years, the global surface DIC database has been greatly expanded, culminating now in GLODAPv2 (Key et al., 2015; Olsen et al., 2016), but the controls producing the global spatial DIC distribution have not been quantitatively reassessed.

Many processes are known to influence the sea surface distribution of DIC at the local scale. They can be divided overall into those which change DIC concentration by direct addition or removal (e.g., 1-3 of the following), and those which affect DIC indirectly (e.g., 4-6 of the following): (1) biological carbon assimilation during primary production and releasing during remineralization (Bozec et al., 2006; Clargo et al., 2015; Toggweiler et al., 2003b; Yasunaka et al., 2013); (2) transport of DIC-rich deep waters into the surface layer (Jiang et al., 2013; Lee et al., 2000); (3) production and export of $CaCO_3$; (4) seawater dilution/concentration due to precipitation/evaporation (Friis et al., 2003); (5) warming or cooling, which alters the CO_2 solubility and induces air-sea gas exchange that acts to reduce air-sea CO_2 disequilibrium (Bozec et al., 2006; Toggweiler et al., 2003a; Williams and Follows, 2011); and (6) the above processes (1-4) through their on TA: if high/low TA values are not matched by high/low DIC values then the resulting low/high seawater pCO_2 stimulates ingassing/outgassing until DIC matches TA (Humphreys, 2017).

Our study differs from previous work in several ways. Firstly, whereas many previous studies looked to understand the vertical DIC distribution, here the target is to understand the horizontal surface DIC distribution. Secondly, we look to identify the most important *processes* not just *variables* driving the surface distribution (Fig. 2). Another difference from previous studies is our use of a much larger observational global dataset – GLODAPv2.

We evaluated the following three main hypotheses as to which processes cause the increase in surface DIC and nDIC from low to high latitudes (Fig. 1):

(1) latitudinal variation of solar heating via its effect on sea surface temperature, and hence CO_2 solubility;

(2) evaporation and precipitation, through their effects on TA; and

(3) upwelling and winter entrainment through the introduction of DIC- and TA-rich deep waters to the (sub)polar surface oceans, when coupled with iron limitation of biological uptake of DIC.

It is easier to constrain the dynamics of upwelling and quantify its impact on surface DIC in the Southern Ocean (where upwelling has been more comprehensively studied, e.g., Marshall and Speer, 2012; Morrison et al., 2015) than in the subarctic North Atlantic and North Pacific Oceans (where upwards transport occurs via deep mixing in the winter, combined with upwelling in the North Pacific). The Southern Ocean also plays a crucial role in the global overturning circulation (e.g., Marshall and Speer, 2012), and the global carbon cycle (Landschützer et al., 2015; Mikaloff-Fletcher, 2015). Therefore, we focused on the Southern Ocean for the evaluation of the third hypothesis.

The processes that we evaluated can be separated into two categories: equilibrium and disequilibrium processes (Fig. 2). The effects of equilibrium processes (the effects through temperature and upwelled TA) change the surface ocean DIC at which air-sea CO_2 equilibrium would occur, and those effects can therefore persist beyond the air-sea CO_2 equilibrium timescale (months to year, Jones et al., 2014). The effects of disequilibrium processes (the effects through direct supply of DIC from upwelling and the effects through biological uptake of DIC in response to upwelled nutrients (principally iron, Moore et al., 2016)), on the other hand, are likely to persist only over timescales shorter than the CO_2 equilibrium timescale. A novel

conclusion of this study is that upwelling, whose global significance has previously been overlooked, is very important in shaping the spatial distribution of surface ocean DIC, in part because upwelling of TA changes equilibrium DIC.

2 Methods

Data for this study were taken from GLODAPv2 (https://www.nodc.noaa.gov/ocads/oceans/GLODAPv2/) (Key et al., 2015; Olsen et al., 2016). This product includes data from over 700 cruises conducted during the years 1972-2013 with a large fraction (~34%) having taken place during the period 2003-2013. These data have been subject to secondary quality control and subsequent adjustments (Key et al., 2015; Lauvset and Tanhua, 2015; Olsen et al., 2016). We define the surface ocean as waters shallower than 30 m at latitudes greater than 30°, and shallower than 20 m at latitudes less than 30° (following e.g., Fry et al., 2015; Lee et al., 2006). Only open ocean data (water depth > 200 m) were included in this study (Fig. 3).

2.1. Data processing

We excluded regions subjected to significant perturbations from river inputs in order to remove confounding factors affecting the latitudinal distributions of DIC and nDIC on smaller length scales than being investigated here. We excluded all data from the Arctic Ocean (> 65° N) (Fig. 3) because they are heavily influenced by river inputs (Fry et al., 2015; Jiang et al., 2014), all data from the Mediterranean Sea and the Red Sea because of its very high salinity (Jiang et al., 2014), as well as some data (those where S is less than 34) from other ocean areas: the Amazon River plume in the North Atlantic (5° N-10° N, > 45° W), the Ganges/Brahmaputra plume in the Bay of Bengal (> 5° N, 80-94° E) (both Fry et al., 2015) and the western North Atlantic margins (Cai et al., 2010). We also excluded relatively small low-latitude ocean areas affected by upwelling (the eastern equatorial Pacific and northern Californian upwelling regions).

Because atmospheric CO_2 increased during the time that the GLODAPv2 data was collected (1972-2013), DIC has also increased in response in surface ocean waters (Bates et al., 2014). To prevent DIC time trends from generating artificial spatial variability, we normalized surface DIC to a reference year of 2005. We assumed that sea surface CO_2 changes track atmospheric CO_2 changes (Feely, 2008; see also CO_2 Time Series in the North Pacific at https://pmel.noaa.gov/co2/file/CO2+time+series). We first calculated the change of atmospheric mole fraction of CO_2 ($xCO_{2,air}$) from the reference year 2005:

$$\Delta xCO_{2,air} = xCO_{2,air}^{t} - xCO_{2,air}^{2005} \tag{2}$$

where the superscript "t" and "2005" refer to year, and the globally averaged atmospheric xCO_2 data can be found at https://www.esrl.noaa.gov/gmd/ccgg/trends/ (neither spatial nor seasonal variability in atmospheric CO_2 is taken into account). Then we converted $\Delta xCO_{2,air}$ into $\Delta pCO_{2,air}$ (Takahashi et al., 2009) just above the sea surface, using in-situ humidity data. It is then assumed that $\Delta pCO_{2,sw}$, representing the change of sea surface pCO_2 relative to the year 2005, is equal to $\Delta pCO_{2,air}$. Therefore the sea surface pCO_2 normalized to year 2005 was calculated as:

$$pCO_{2,sw}^{2005} = pCO_{2,sw}^{t} - \Delta pCO_{2,sw} \qquad\qquad (3)$$

where $pCO_{2,sw}^{t}$ was calculated from in-situ DIC, TA, temperature and salinity through CO_2SYS (van Heuven et al., 2011; dissociation constants used are described in Sect. 2.3).

Since the anthropogenic CO_2 perturbation does not change TA, DIC normalized to 2005 was calculated with inputs of in-situ

5   TA and $pCO_{2,sw}^{2005}$ using CO_2SYS (van Heuven et al., 2011):

$$DIC^{2005} = f(T_{in\text{-}situ}, S_{in\text{-}situ}, TA_{in\text{-}situ}, pCO_{2,sw}^{2005}) \qquad\qquad (4)$$

The concentration of DIC hereinafter refers to the DIC normalized to year 2005.

2.2 Salinity normalization

Salinity normalization was used to correct for the influence of precipitation and evaporation in the open ocean (Postma, 1964).

10   Data were normalized to a reference salinity of 35 using a standard procedure:

$$nX = X_{obs} \times 35/S_{obs} \qquad\qquad (5)$$

where nX refers to the normalized variable, X_{obs} is the observed value of the variable, and S_{obs} is the observed salinity.

It should be acknowledged that straightforward salinity normalization (Eq. 5) can create artificial variance in DIC distribution (Friis et al., 2003) because it ignores the influences of riverine input and upwelling from below the lysocline. To this end, we

15   excluded the major regions affected by river inputs (see text in Sect. 2.1). In addition, we found that the influence of upwelling from below the lysocline on salinity normalization of DIC is negligible (i.e., it can only account for up to 4 µmol kg^{-1} artificial change in DIC) compared with the DIC latitudinal gradient of about 200 µmol kg^{-1} that we seek to explain in this study.

2.3 Carbonate chemistry

Carbonate system variables were calculated from DIC and TA using version 1.1 of CO_2SYS for MATLAB (van Heuven et al.,

20   2011). The dissociation constants for carbonic acid and sulfate were taken from Lueker et al. (2000) and Dickson (1990), respectively, and the total borate-salinity relationship from Lee et al. (2010).

2.4 Calculations of the effects of various processes on DIC

The second hypothesis (evaporation and precipitation through their effects on TA) was evaluated by salinity normalization (Eq. 5). The methods for calculating the impacts of the other two processes on the surface DIC concentration are now explained

25   The effect of upwelling is evaluated in the Southern Ocean, from both short- and long-term perspectives. In addition, we also quantify the effect of iron limitation, which would potentially affect the observed (n)DIC distribution.

2.4.1 SST-driven effect

Generally, the temperature effect on the carbonate system has two aspects. Firstly, when water temperature increases, the equilibrium between carbonate species (Eq. 6) shifts to the left, increasing the aqueous CO_2 and carbonate ion concentrations (Dickson and Millero, 1987):

5    $$CO_2 + H_2O + CO_3^{2-} \rightleftharpoons 2HCO_3^- \qquad (6)$$

Secondly, CO_2 solubility is reduced at higher temperatures and vice versa (Weiss, 1974). Neither effect alters DIC directly but both lead to changes in pCO_2. A larger proportion of DIC exists as aqueous CO_2 at higher temperatures and the ratio of pCO_2 to $[CO_2]$ also increases as solubility decreases (Eq. 7, Henry's Law):

$$pCO_2 = [CO_2]/K_H \qquad (7)$$

10   where K_H is the Henry's constant (solubility) for CO_2, one of the CO_2 system equilibrium constants.

Both effects thus tend to increase sea surface pCO_2 as sea water warms, potentially elevating it to values above the atmospheric pCO_2 and thereby stimulating air-sea CO_2 gas exchange; the induced outgassing of CO_2 reduces sea surface CO_2 and DIC as it shifts the system towards air-sea CO_2 equilibrium. Therefore, for an open ocean system with gas exchange with the atmosphere, the DIC distribution has the potential to be controlled by the SST distribution, and this can by itself produce DIC

15   latitudinal variations.

To examine the magnitude of the expected temperature-induced DIC changes, we chose the low-latitude area as the reference, then removed the latitudinal SST variation and recalculated the open ocean surface DIC everywhere for a constant SST of 27°C (the mean sea surface temperature in the subtropics 30° S-30° N). To do this we first calculated the in-situ pCO_2 from observed SST, SSS (sea surface salinity), TA and DIC using CO_2SYS. The calculated pCO_2 from TA and DIC has been found

20   to agree well with the measured pCO_2 (root mean square deviation of $\pm$ 6.8 μatm, Takahashi et al., 2014). We then altered the sea surface temperature from its in-situ value to 27°C, which would change the solubility of CO_2 and induce air-sea CO_2 gas exchange. Then air-sea CO_2 gas exchange (which does not change TA) was assumed to proceed until pCO_2 was back to the same level as before resetting the temperature. Next, we used CO_2SYS to calculate $DIC_{SST=27}$ based on an input temperature of 27°C, observed salinity and TA, and the in-situ pCO_2 calculated as above. $DIC_{SST=27}$ thus represents temperature-normalized

25   DIC, and should exhibit the same spatial variability as DIC except that the temperature-induced component of the variability has been removed. Finally, the difference between observed DIC and $DIC_{SST=27}$ gives the DIC variation attributed to temperature variation:

$$\Delta DIC_{temp} = DIC_{obs} - DIC_{SST=27} \qquad (8)$$

2.4.2. Upwelled DIC-driven effect (short-term effect of upwelling)

30   Upwelling of DIC-rich subsurface water is capable of increasing the surface DIC. The largest upwelling (in terms of flow rate) anywhere in the world takes place in the Southern Ocean (Talley, 2013): the upwelling there is made up of 18 Sv (Sverdrup, 1 Sv = 10^6 m³/s) of NADW (North Atlantic Deep Water), 11 Sv of IDW (Indian Deep Water), and 9 Sv of PDW (Pacific Deep

Water). Subsurface waters in the Southern Ocean are considered to upwell along the neutral density isopycnals of 27.6 kg m^{-3}, 27.9 kg m^{-3} and 27.9 kg m^{-3} in the southern Atlantic, Indian and Pacific Oceans, respectively (Ferrari et al., 2014; Lumpkin and Speer, 2007; Marshall and Speer, 2012; Talley, 2013).

Upwelling occurs within the Antarctic Circumpolar Current (ACC) at those latitudes where the wind stress is greatest (Morrison et al., 2015); as the upwelled water subsequently advects away, the effects are transported to nearby locations. Therefore, instead of a direct supply from deep to surface locations such as L3 (Fig. 4), DIC is assumed to be brought to the subsurface primarily along isopycnals (shown in Fig. 4 as the black curve to L1), finally reaching the surface at L2, the zone in which upwelling occurs. Then, the upwelled subsurface water with enriched DIC, TA and nutrients feeds both branches of the overturning in the Southern Ocean. One is transported northwards via Ekman transport from L2 to L3 to join the upper branch, as shown by the black arrow towards the equator, and the other one is recycled back through the lower branch to form Antarctic Bottom Water (AABW) (Talley, 2013). Potential effects of upwelling on sea surface temperature are not considered here, but are likely to be small because both deep water and high-latitude surface waters are cold.

We first consider the increase in DIC induced by the upwelling of deep water with high DIC concentrations. While some of the initial increase is usually removed shortly afterwards by biological export fueled by the nutrients brought up at the same time, excess DIC remains if the subsequent biological removal of DIC does not match the initial increase. Phosphorus has the simplest nutrient behavior in the ocean with only one significant source to the ocean as a whole (river input) and one major sink (organic matter burial) (Ruttenberg, 2003; Tyrrell, 1999). In this study, the salinity-normalized phosphate (nPhos) concentration was used as a proxy for calculating how much salinity-normalized DIC (nDIC) was upwelled along with it and not yet removed again by biological uptake of phosphate and DIC. We used salinity-normalized concentrations to correct for the influence of precipitation (rainfall) that dilutes DIC and phosphate concentrations in proportion to the effects on salinity (Eq. 5). In this calculation, it was assumed that the only external source of phosphate to surface waters is from upwelling and the only subsequent loss is through export of organic matter, leading to the equation:

$$nPhos_{surf} = nPhos_{supply} - NCP/R_{C:P} \qquad (9)$$

where the subscript 'supply' indicates the end-member concentration of deep water supplied along the upwelling isopycnals (i.e., the value at L1 in Fig. 4), and the subscript 'surf' indicates the surface water concentration at some later time. NCP refers to the total time-integrated net community production (uptake and export by biology) in carbon units, and $R_{C:P}$ is the Redfield ratio of carbon to phosphorus. $R_{C:P}$ is given the standard value of 106:1 (Redfield, 1963), except for the cold nutrient-rich high-latitude region in the Southern Ocean (south of 45° S), where $R_{C:P}$ is given a lower value, of 78:1 (Martiny et al., 2013). $nPhos_{surf}$ refers to the observed surface value of nPhos at some location distant from where upwelling occurs.

Another possible process involved in the change of DIC during its upwelling and subsequent advection is calcium carbonate (CaCO$_3$) precipitation and dissolution (Balch et al., 2016), which alters DIC and TA with a ratio of 1:2. In order to quantify the magnitude of this process, we used Alk* (Fry et al., 2015) as an indicator, which is capable of diagnosing CaCO$_3$ cycling in the context of the large-scale ocean circulation (see more details on Alk* distribution in Fig. 10). The change in Alk*

concentrations between its supplied and surface end-members is attributed to $CaCO_3$ precipitation/dissolution and assimilation of inorganic nutrients by primary production (Brewer and Goldman, 1976):

$$Alk_{surf}^* = Alk_{supply}^* - \Delta Alk_{CaCO3}^* - NCP/R_{DIC:TA} \tag{10}$$

$$Alk^* = \frac{Alk_m - Alk_r + 1.36 \times NO_3^-}{S} \times 35 + Alk_r - 2300 \text{ µmol kg}^{-1} \tag{11}$$

where $R_{DIC:TA}$ is the relative ratio of -106/17 between changes in DIC and TA during primary production (Wolf-Gladrow et al., 2007). Alk_m is the measured TA, Alk_r is the riverine TA end-member (zero in the Southern Ocean), and 2300 µmol kg^{-1} is the average TA in the low-latitude surface oceans. Alk_{surf}^* is calculated by Eq. 11.

Assuming the carbon source is from upwelled CO_2-rich deep waters and carbon sinks are from organic matter export (NCP) and $CaCO_3$ cycling, then:

$$nDIC_{surf} = nDIC_{supply} - NCP - 0.5 \times \Delta Alk_{CaCO3}^* \tag{12}$$

Three hydrographic sections, one in each of the Indian (I95E), Pacific (P150W), and Atlantic (A25W) Oceans, were used to determine the different supply concentrations ($nPhos_{supply}$, Alk_{supply}^* and $nDIC_{supply}$) for each basin (see Fig. 5c inset, values here are expressed as mean ± standard error of the mean). In the Indian Ocean, $nPhos_{supply}$, Alk_{supply}^* and $nDIC_{supply}$ along the 27.9 kg m^{-3} isopycnal are. 2.29 ± 0.01 µmol kg^{-1}, 109.4 ± 1.0 µmol kg^{-1}, and 2273.1 ± 1.1 µmol kg^{-1}, respectively, as it approaches the surface. In the Pacific Ocean, $nPhos_{supply}$, Alk_{supply}^* and $nDIC_{supply}$ along the 27.9 kg m^{-3} isopycnal are 2.32 ± 0.01 µmol kg^{-1}, 108.1 ± 1.9 µmol kg^{-1}, and 2277.2 ± 1.8 µmol kg^{-1}, respectively. In the Atlantic Ocean, $nPhos_{supply}$, Alk_{supply}^* and $nDIC_{supply}$ along the 27.6 kg m^{-3} isopycnal are 2.28 ± 0.01 µmol kg^{-1}, 103.5 ± 1.1 µmol kg^{-1}, and 2254.6 ± 1.3 µmol kg^{-1}, respectively (Fig. 5).

Since $nPhos_{surf}$ tends to decrease to zero upon moving northwards, due to biological uptake, $nDIC_{surf}$ has a relatively constant value in the subtropical regions (data not shown), where is not influenced by upwelling in the Southern Ocean. Because of this, the potential effect of upwelling on surface nDIC, is calculated as the excess in $nDIC_{surf}$ compared to the subtropical average value (30° S-30° N):

$$\Delta nDIC_{upw\_st} = nDIC_{surf} - \overline{nDIC_{surf} \ (30° S\text{-}30° N)} \tag{13}$$

2.4.3. Upwelled TA-driven effect (long-term effect of upwelling)

Some effects of upwelling on DIC are temporary, becoming overridden later by gas-exchange. In contrast, the effect of upwelled TA persists because it changes the equilibrium DIC with respect to gas exchange (DIC_{eq}) (discussed also in Sect. 4.1.3). Upwelling of high-TA water has a long-lasting effect on DIC because, if all else remains constant, an increase in TA decreases the fraction of DIC that exists as CO_2 molecules. The resulting decrease in CO_2 concentration lowers seawater partial pressure of CO_2 (pCO_2), having the potential to lower seawater pCO_2 to below atmospheric values which in turn drives an influx of CO_2 from the atmosphere, raising DIC (Humphreys et al., 2017).The effects of upwelling are complex because they consist of both direct and indirect effects on DIC (Fig. 2), lasting over both short (when DIC is altered but DIC_{eq} is not) and long (when DIC_{eq} is altered) timescales. The different effects and the meanings of the terms used here are illustrated in Fig. 6.

The calculation of the long-term effect of upwelling through upwelled TA in the Southern Ocean (i.e., the difference between DIC_3 and DIC_0 in Fig. 6) was achieved through five steps:

(1) calculation of TA in the Southern Ocean with the upwelling effect subtracted, TA_{nonupw}:

$$TA_{nonupw} = TA_{obs} - (Alk^* \times S_{obs} / 35) \tag{14}$$

where TA_{obs} is the observed in-situ TA, and Alk^* is the TA tracer (Fry et al., 2015) revealing excess TA supplied by the large-scale ocean circulation (upwelling in the Southern Ocean), as well as removal by calcification and export (Eq. 11). Since Alk^* is a salinity-normalized concept, it is necessary to restore it to the in-situ salinity before subtracting it from the in-situ TA.

(2) calculation of in-situ sea surface pCO_2, following the same method as described in Sect. 2.4.2.

(3) calculation of DIC with the effect of upwelled TA subtracted. We calculated DIC_{nonupw} using CO_2SYS with inputs of TA_{nonupw} and in situ pCO_2, SST and salinity.

(4) salinity-normalization for consistency with other calculated effects.

(5) finally, the long-term effect of upwelling through the upwelled TA and the subsequent air-sea gas exchange is calculated as:

$$\Delta nDIC_{upw\_lt} = nDIC_{obs} - nDIC_{nonupw} \tag{15}$$

where $\Delta nDIC_{upw\_lt}$ corresponds to the magnitude of ⑤ in Fig. 6.

2.4.4. Iron-driven effect

The iron limitation-driven DIC differences (ΔDIC_{Fe}) relate to the concepts of "unused nutrient" and associated "unused DIC", which can be thought of as the amounts of macro-nutrients and DIC that are left behind after iron limitation brings an end to biological uptake, in those regions where iron is the limiting nutrient. Iron limitation alters the impact of upwelling. In locations experiencing upwelling but where nitrate is the proximate limiting nutrient, then the quantity of upwelled DIC might more or less balanced by the quantity of subsequently exported DIC (fueled by the upwelled nitrate). In the Southern Ocean, however, the two appear not to be close to balance, even before considering iron limitation. According to the calculations in Sect. 2.4.2, the ratio of the excess upwelled nDIC against nPhos is around $250:2.3 \approx 109:1$ for the Southern Ocean, considerably exceeding the low C:P (average $\approx 80:1$) of organic matter in the region (Martiny et al, 2013). So even if all upwelled phosphate were to be used up and then exported in biomass in conjunction with carbon, a considerable surplus of DIC would be left behind. A lack of iron in surface waters, however, leads to even more upwelled DIC being left behind after the end of blooms induced by the upwelled nutrients.

We used phosphate as the "unused nutrient" from which to calculated "unused DIC".

For each $1° \times 1°$ grid in the surface open ocean, the unused phosphate was taken from its annual minimum concentration based on the monthly data in World Ocean Atlas 2013 version 2 (WOA 2013: https://www.nodc.noaa.gov/OC5/woa13/, Boyer et al., 2013). The unused phosphate was then converted into unused DIC based on a C:P ratio of 106:1 (Redfield, 1963) for most of the global ocean, except in the warm nutrient-depleted low-latitude gyres, warm nutrient-rich equatorial upwelling regions,

and cold nutrient-rich high-latitude regions. The C:N ratios used for these three regions were 195:1, 137:1, and 78:1, respectively (Martiny et al., 2013).

The amount of unused DIC was therefore calculated as:

$$\text{unused DIC} = \text{unused phosphate} \times R_{C:P} \tag{16}$$

2.5. Uncertainty estimation

In this study, uncertainties in calculated effects of different drivers (e.g., $\Delta nDIC_{temp}$, $\Delta nDIC_{upw\_st}$, $\Delta nDIC_{upw\_lt}$) were determined by a Monte Carlo approach. For example, the uncertainty of $\Delta nDIC_{temp}$ was calculated as follows: (1) given that $\Delta nDIC_{temp}$ is the difference between $nDIC_{obs}$ and $nDIC_{SST=27}$ (Eq. 9), its uncertainty is propagated from the uncertainties of both $nDIC_{obs}$ and $nDIC_{SST=27}$, where the uncertainty of $nDIC_{obs}$ is 5 µmol kg^{-1} (Table 2), and the uncertainty of $nDIC_{SST=27}$ was determined by a Monte Carlo approach; (2) for calculation of the uncertainty of $nDIC_{SST=27}$ (see its function in Table 1), we first calculated artificial random errors (normally distributed according to the central limit theorem, with a mean of zero and a standard deviation equal to the accuracy/uncertainty of measurement) using a random number generator. Then, new carbonate system variable values (the original ones plus the randomly generated errors) were input into the CO$_2$SYS program (Van Heuven et al., 2011) to calculate new $nDIC_{SST=27}$ values. By doing this 1000 times, we obtained a set of 1000 different values for every single data point in the dataset. We used the standard deviations of these sets to characterize their individual uncertainties. The overall uncertainty of $nDIC_{SST=27}$ was 6.4 µmol kg^{-1}; (3) by applying the same Monte Carlo method, but to calculate the uncertainty propagated through Eq. (9), we then calculated the uncertainty of $\Delta nDIC_{temp}$ to be 8.0 µmol kg^{-1} (Table 2).

This Monte Carlo approach has been used previously (e.g., Juranek et al., 2009; Ribas-Ribas et al., 2014) to propagate uncertainties involving CO$_2$ system calculations.

3. Results

3.1. Spatial distributions of DIC and nDIC

Surface observations reveal values of DIC across the global ocean ranging from less than 1850 µmol kg^{-1} in the tropics to more than 2200 µmol kg^{-1} in the high latitudes (Fig. 1a). To first order, surface DIC increases polewards, being positively correlated with absolute latitude (Spearman's rank correlation coefficient $\rho = 0.71$ for the global oceans, Table 3). Spatially, it is monotonically inversely related to sea surface temperature ($\rho = -0.78$, Table 3), with DIC being highest where the surface ocean is coolest. Another conspicuous feature of surface DIC is the higher values (by ~100 µmol kg^{-1}) in the tropical and subtropical Atlantic Ocean relative to the same latitudes in the Pacific and Indian Oceans (Fig. 1a), as attributed to the transport of water vapor from the Atlantic to the Pacific (Broecker, 1989). This is not considered further here because our main purpose is to explain the sizeable observed latitudinal gradients in DIC (on average 153 µmol kg^{-1} higher in the Southern Ocean than at low latitudes, for instance) and nDIC (on average 223 µmol kg^{-1} higher in the Southern Ocean than at low latitudes).

Salinity-normalized DIC (nDIC) increases towards the poles in all three ocean basins (Fig. 1b), although less strongly in the North Atlantic. The surface nDIC correlates more tightly with latitude and SST than does DIC, yielding a positive correlation with absolute latitude and a negative correlation with SST ($\rho = 0.86$ and -0.94 respectively for the global ocean, Table 3). The distributions of surface DIC and particularly nDIC also show modest regional maxima in the eastern equatorial Pacific,

5 the Arabian Sea, and the eastern boundaries of the Pacific and Atlantic Ocean basins, presumably as a result of upwelling (Capone and Hutchins, 2013; Chavez and Messié, 2009; Millero et al., 1998; Murray et al., 1994).

3.2. SST-driven effect in the global surface ocean

The differences between the latitudinal patterns of DIC_{obs} and $DIC_{SST=27}$ are shown in Fig. 7. As expected, $DIC_{SST=27}$ agrees well with DIC_{obs} in the subtropics where SST is close to 27°C; the differences become larger with increasing latitude and

10 decreasing SST (Fig. 7a-c). Correcting for salinity variations (Fig. 7d-f) greatly reduces the variability in DIC at low latitudes: $nDIC_{obs}$ is fairly constant at ~1970 µmol kg^{-1} in the subtropics. $\Delta nDIC_{temp}$ (Eq. 8 but for nDIC), the temperature-driven CO_2 gas exchange effect on surface nDIC, increases sharply with latitude (Fig. 7g-i), reaching ~220 µmol kg^{-1} at 70° S, and ~200 µmol kg^{-1} at 60° N in the northern part of the Atlantic and Pacific Oceans, with an average value of 182 µmol kg^{-1} in the Southern Ocean, which is large enough to account by itself for most - but not all - of the nDIC latitudinal gradient of 223 µmol

15 kg^{-1} (2193-1970 µmol kg^{-1}).

The estimated overall uncertainty of SST-driven effect on surface nDIC (Table 2) ranges from 5 to 8 µmol kg^{-1}, which is of comparable magnitude to the uncertainty of DIC normalized to 2005, and much smaller than the large latitudinal variations of $\Delta nDIC_{temp}$.

3.3. Upwelling-driven effect in the Southern Ocean

20 The upwelling-driven effects in the Southern Ocean calculated from both short- and long-term perspectives are shown in Fig. 8.

$\Delta nDIC_{upw\_st}$ increases polewards (Fig. 8a-c), with the same trends as surface phosphate (not shown), because it is calculated from phosphate. It can be seen that surface nDIC is potentially elevated dramatically by the Southern Ocean upwelling. The effect is of larger magnitude (average of 220 µmol kg^{-1} in the Southern Ocean) than that calculated for $\Delta nDIC_{temp}$ (Fig. 7g-i).

25 Fig. 8d-f show the long-term effect of upwelling, which are controlled by the concentration of TA in the upwelled water (how much upwelling increases surface TA values by). The average magnitude of $\Delta nDIC_{upw\_lt}$ is around 74 µmol kg^{-1} for the Southern Ocean.

The estimated overall uncertainty of upwelling-driven effects on surface nDIC (Table 2) ranges from 5 to 9 µmol kg^{-1}, close to the uncertainty of DIC normalized to 2005, and much smaller than the large latitudinal variations of $\Delta nDIC_{upw\_st}$ and

30 $\Delta nDIC_{upw\_lt}$.

3.4. Iron-driven effect in the global surface ocean

As shown in Fig. 9, ΔDIC_{Fe} is close to zero except in the classic HNLC regions (i.e., the North Pacific, the equatorial Pacific, and the Southern Ocean, Moore et al., 2013). There is also some residual nitrate during most summers in the Iceland and Irminger Basins of the North Atlantic due to the seasonal iron limitation there (Nielsdóttir et al., 2009). The surface Southern Ocean south of 40° S has the largest unused DIC (ΔDIC_{Fe} of up to 180 µmol kg^{-1}, average of 120 µmol kg^{-1}), followed by the North Pacific 40° N-65° N (ΔDIC_{Fe} of up to 120 µmol kg^{-1}, average of 75 µmol kg^{-1}) and the equatorial Pacific (average of 35 µmol kg^{-1}). It is negligible elsewhere in the tropics and subtropics.

4. Discussion

4.1. Factors controlling the surface DIC latitudinal variation

4.1.1. Effect of SST variation in the global surface ocean

The previously accepted explanation for higher DIC at high latitudes is that cooler SSTs there increase CO_2 solubility, resulting in a higher equilibrium DIC (Toggweiler et al., 2003a; Williams and Follows, 2011). Our results support an important role for SST, but also that other processes contribute significantly.

Our analysis concludes that the latitudinal gradient in temperature is capable of raising nDIC by about 180 µmol kg^{-1} in the Southern Ocean, or in other words of explaining about four-fifths of the observed gradient of 223 µmol kg^{-1}. SST variation is thus able to explain most of the observed pattern.

4.1.2. Effect of TA distribution in the global surface ocean

A second factor that has been proposed as influential in driving spatial variations in the concentration of DIC in the surface ocean is TA (Williams and Follows, 2011). Our analysis supports this contention, although we note that the effect of TA is most prominent at low latitudes. Large differences in DIC are observed between the subtropical gyres, where values are relatively high, and the vicinity of the equator, where values are relatively low (Fig. 1a). These differences are driven by the effects of evaporation and precipitation on TA, which then drive differences in DIC because of the influence of TA on DIC at gas exchange equilibrium with a given atmospheric CO_2 level. The role of TA explains the much clearer relationship between latitude and nDIC than between latitude and DIC (Fig. 1, Table 3); normalizing DIC to salinity is almost the same as normalizing DIC to TA, because salinity and TA are highly correlated in the surface ocean. As a result, the effect of TA on DIC is counteracted by salinity normalization, with the pattern in nDIC (Fig. 1b) then revealing more clearly how other factors impact DIC.

The latitudinal pattern in TA is not the dominant driver of the DIC trend, because TA values are generally lower at high latitudes (where precipitation often exceeds evaporation) than they are at low latitudes (where evaporation often exceeds

precipitation). However, TA is also biologically cycled and thus not perfectly correlated to salinity (Fry et al., 2015) and the presence of excess TA in deep water upwelled at high latitudes does contribute to the DIC trend.

4.1.3. Effect of upwelling in the Southern Ocean

Although not traditionally considered as a factor, our analyses show that upwelling is important in driving the latitudinal
5   gradient in DIC. Upwelling of DIC by itself is capable of producing an nDIC latitudinal gradient of 220 µmol kg^{-1} in the Southern Ocean, even higher than the effect of temperature (Fig. 8a-c, Table 4). However, the contribution of upwelling is reduced by about two thirds if only the long-term effect through upwelled TA is considered (see Fig. 6 for definitions of terms). Deep water usually has higher concentrations of nutrients, DIC and nTA than does surface water. Introduction of deep water into the surface mixed layer therefore usually stimulates increases in these concentrations, with three main consequences for
10   DIC (Fig. 6), as follows. (A) If the upwelled water has higher DIC than the surface then the upwelling causes an immediate initial increase in DIC; (B) additional nutrients stimulate phytoplankton blooms until the proximate limiting nutrient runs out, leading to a reduction in DIC over timescales of days to weeks (or months if, for instance, the upwelling occurs at high latitudes during winter when phytoplankton cannot bloom); (C) finally, air-sea gas exchange tends to remove any upwelling-induced air-sea CO_2 disequilibrium over a period of months to a year (Jones et al., 2014), although the full equilibrium is seldom
15   achieved across the global surface ocean (Takahashi et al., 2014).

The upwelling effects in Fig. 8 are calculations based on phosphate and TA concentrations, taking into account both the amount upwelled, and the amount subsequently removed by biology. They therefore correspond to the sum of the direct upwelling effect (① in Fig. 6) and the indirect upwelling effect through supplied nutrients (② in Fig. 6). There are two reasons why the initial amount of upwelled DIC considerably exceeds the amount of DIC subsequently taken up by phytoplankton growth
20   fueled by the upwelled nutrients (why ① > ②) in the Southern Ocean.

Firstly, iron is typically much scarcer in deep waters than are macronutrients, relative to phytoplankton need (Moore, 2016). Regions like the Southern Ocean that are strongly influenced by upwelling are for this reason often iron-limited (Moore, 2016), leading to large amounts of 'unused DIC' (order of 120 µmol kg^{-1} in the Southern Ocean - Fig. 9) accompanying unused macronutrients. This scarcity of iron also leads to muted seasonal cycles of DIC (Merlivat et al., 2015) and thus year-round
25   persistence of unused DIC. Secondly, as described in Sect. 2.4.5, the higher C:P ratio of supply (~109:1) compared to removal (~80:1) implies a considerable surplus of DIC even without iron limitation.

The upwelling effects shown in Fig. 8a-c are however relatively short-term, and are expected to be overridden by air-sea gas exchange within months (Jones et al., 2014). They are thus likely to be most significant in the vicinity of where upwelling takes place (Morrison et al., 2015). For effects that may persist further away from locations of upwelling, it is important to
30   consider also the long-term effect (⑤ in Fig. 6), the magnitude of which is dictated mainly by the change in TA brought about by upwelling. The level of TA in upwelled water (~2315, 2340, and 2337 µmol kg^{-1} in the Atlantic, Indian and Pacific sectors of Southern Ocean, respectively; calculated according to the same method as in Sect. 2.4.3) are higher than the typical levels of TA in the surface waters of the high latitude Southern Ocean (~2300, 2289, and 2288 µmol kg^{-1} in the Atlantic, Indian and

Pacific sectors, respectively). The increase in TA brought about by upwelling corresponds to a long-term upwelling effect on nDIC of about 74 µmol kg^{-1} (Fig. 8d-f) in the Southern Ocean.

Our results show that upwelling in the Southern Ocean can, by itself, generate high-latitude nDIC values that are around 220 µmol kg^{-1} greater than subtropical values. We emphasize that there is, in addition, a sizeable long-term effect of upwelling
5 (forcing nDIC values to be around 74 µmol kg^{-1} higher than they would be otherwise). Contrary to what might typically be assumed, the long-term effects of upwelling are dictated by the amounts of TA upwelled, and not by the amounts of DIC or nutrients.

4.2. A new understanding of the controls on the surface DIC distribution

The analyses presented above show that our understanding of the causes of latitudinal gradient in DIC needs to be revised.
10 Whereas it was considered previously that the latitudinal gradient in DIC is completely explained by sea surface temperature variation, here we have shown that upwelling is also an important contributor to it, based on an evaluation in the Southern Ocean. DIC and nDIC would still be elevated at high latitudes even if there was no temperature effect (even if CO_2 solubility was completely unaffected by SST). The incomplete previous view of what drives the DIC latitudinal gradients should be replaced by this more nuanced view in which upwelling is also seen to contribute.

15 It seems that neither temperature variation nor upwelling are responsible for all of the observed large latitudinal gradients in DIC and nDIC (for instance, the ~223 µmol kg^{-1} difference in nDIC between low-latitudes and the Southern Ocean), but rather that they are jointly responsible. There is an apparent contradiction because both $\Delta nDIC_{temp}$ and $\Delta nDIC_{upw\_st}$ appear to account for more than 80% of the nDIC latitudinal gradient. While both processes are capable individually of raising DIC by 182 and 220 µmol kg^{-1} in the Southern Ocean, acting together they raise it by only 223 µmol kg^{-1} instead of 400 µmol kg^{-1}. An obvious
20 explanation of this apparent paradox is that when we consider upwelling effects, we should consider not only its short-term effect through supplying DIC and nutrients (① + ② in Fig. 6), but also its long-term effect with gas exchange with the atmosphere (⑤ = ① + ② + ③ in Fig. 6), the amount of which is a function of the amount of upwelled TA (which, together with temperature, controls the equilibrium DIC).. The sum of the SST-driven effect and the long-term effect of upwelling approximately equals the nDIC latitudinal gradient (Table 4).
25 On the global scale, therefore, the ultimate controls on the surface DIC and nDIC latitudinal gradients are the spatial patterns of SST and upwelling, and the chemical composition of the upwelled water.

4.3. Importance of upwelling confirmed by the North Atlantic

From inspection of the global nDIC distribution (Fig. 1b), it can be seen that nDIC increases with latitude in all basins, but, as shown in Table 4, does so less strongly in the North Atlantic (difference between high latitudes and low latitudes of 114 µmol
30 kg^{-1}) than in the North Pacific (difference of 192 µmol kg^{-1}). Although the latitudinal temperature gradient is less pronounced in the North Atlantic, this is not enough to explain the variation in gradients between the two basins: the average temperature

of the high-latitude North Atlantic is 12.4°C and of the high-latitude North Pacific is 9.5°C, which can explain about 20 μmol kg^{-1} of variation between the two nDIC gradients but cannot explain the observed 78 μmol kg^{-1} variation (Table 4).

The reason for the discrepancy is that the Southern Ocean and the North Pacific experience elevations in values due to inputs of deep water whereas the North Atlantic does not. Upwelling occurs in the Southern Ocean and entrainment due to deep winter mixing occurs in the subarctic North Pacific (Mecking et al., 2008; Ohno et al., 2009) where it entrains waters high in both TA (Fry et al., 2016) and DIC. While deep winter mixing also occurs in the high latitude North Atlantic (de Boyer Montégut et al., 2004), the entrained waters left the surface relatively recently and hence there is little accumulated remineralized DIC and TA in the deep water that is reintroduced to the surface. For this reason, winter entrainment produces little increase in surface nDIC in the North Atlantic. This makes the North Atlantic useful in discriminating between the two effects because, uniquely out of the three regions, only the SST effect operates there. As expected, the SST effect is able to completely account for the observed nDIC gradient in the North Atlantic, whereas it cannot in the other two regions (columns 2 and 3 of Table 4). The North Atlantic confirms the important contribution of upwelling to latitudinal gradients, while also showing that latitudinal gradients occur in the absence of upwelling.

4.4. Comparison of nDIC distribution to Alk* and nutrients

Fig. 10 shows a comparison between the patterns of nDIC, the TA tracer Alk* (Eq. 11, Fry et al., 2015) and salinity-normalized nutrients. The similarities and differences in distributions of Alk* and nutrients have previously been discussed by Fry et al. (2015). Here we extend the comparison to also include nDIC. All exhibit low and fairly constant values at low latitudes, primarily due to biological uptake and restricted supply from subsurface waters, for most variables, but primarily due to fairly uniform high temperatures for nDIC. All increase polewards due to upwelling/entrainment (also SST for nDIC), exhibiting maxima at high latitudes in the Southern Ocean and North Pacific. All exhibit a more modest increase in the North Atlantic than in the North Pacific, because the deep water formed relatively recently. The coincident increases in nDIC and nitrate in the north Indian Ocean and equatorial Pacific Ocean are not matched by increases in either Alk* or silicate, most probably due to the source waters for the upwelling coming from depths that are shallower than the dissolution depths of calcium carbonate and opal (Fry et al., 2015; Schlitzer, 2000). There are differences in the latitudes at which the different parameters start to increase on a transect from the equator towards Antarctica, reflecting the different processes involved. Surface nDIC is the first to start increasing, under the influence of SST (rows 3 and 4 of Fig. 7), at around 20° S in the Atlantic and Pacific Oceans and 25° S in the Indian Ocean. Alk* and nitrate, on the other hand, do not start to increase until about 40° S in the Atlantic and Indian Oceans and about 30° S in the Pacific Ocean. Silicate does not increase in concentration until about 50° S, for reasons that are still debated (Assmy et al., 2013; Holzer et al., 2014; Vance et al., 2017).

4.5. Implications for the future CO₂ sink under climate change

It is widely understood that global warming may alter the spatial distribution and intensity of upwelling in the ocean (Bakun, 1990; McGregor et al., 2007; Wang et al., 2015). It could either increase it on average, due to higher average wind speeds in a warmer, more energetic atmosphere (Bakun, 1990; Wang et al., 2015), or decrease it on average, due to enhanced stratification as the temperature differential between surface and deep waters is increased (Barton et al., 2013; Sarmiento et al., 2004b). Furthermore, it is widely understood that an increase in upwelling would lead to an increase in the amount of CO_2 outgassed from the ocean, as larger quantities of CO_2-rich deep water are brought up to the surface and their CO_2 vented to the atmosphere (Evans et al., 2015; Marinov et al., 2006; Morrison et al., 2015). However, we have identified an additional effect here. Changes in upwelling would alter the distribution of carbon in the surface ocean not only through the supply of CO_2, but also through the supply of TA which determines the eventual surface carbonate system equilibrium with the same atmospheric pCO_2 (Humphreys et al., 2018). That is to say, the impact of changes in upwelling on the ocean's carbon source/sink strength depends not only on the DIC content of the upwelled water but also on its TA content. Ocean carbon cycle models should include these additional consequences if they are to make accurate predictions about the impacts of global warming on future carbon cycling. They should include the several routes identified here by which upwelling affects surface DIC: through upwelling of DIC, through upwelling of nutrients, and through upwelling of TA.

5. Conclusions

We investigated the global surface DIC and nDIC distributions in order to explain the large differences between high latitude (especially Southern Ocean) and low-latitude regions. This issue has been addressed in previous studies and here we revisited it using new analytical approaches that lead to new findings. We considered three drivers for how the phenomenon could be explained: (1) sea surface temperature variations through their effect on CO_2 system equilibrium constants, (2) salinity-related TA variations through their effect on pCO_2, and (3) upwelling in the subpolar oceans. Our analyses confirmed that temperature plays a dominant role through its effect on solubility, and is able to explain a large fraction of the surface nDIC latitudinal gradient (182 μmol kg^{-1} out of 223 μmol kg^{-1} in the high-latitude Southern Ocean). Variations in TA associated with evaporation and precipitation are unable to explain higher DIC concentrations at higher latitudes, because alone they would drive the opposite DIC pattern. Their role is therefore to reduce the magnitude of the polewards gradient in DIC. Upwelling, whose role in driving the large-scale spatial patterns has not previously been appreciated, accounts for a sizeable component of the surface nDIC latitudinal gradient (on average 220 μmol kg^{-1} in the Southern Ocean). Its importance is magnified by the iron limitation that frequently occurs in upwelling areas, leaving behind residual upwelled excess DIC and macronutrients that cannot be utilized by biology. We emphasize that the upwelling of TA alongside DIC generates a prolonged effect that persists beyond CO_2 gas exchange re-equilibration timescales. The long-term effect of upwelling (74 μmol kg^{-1} in the Southern Ocean) helps explain the shortfall between the observed nDIC latitudinal gradient (223 μmol kg^{-1}) and the magnitude of the

temperature-driven effect (182 μmol kg^{-1}). On the global scale, we conclude that no single mechanism accounts for the full amplitude of surface DIC latitudinal variations but that temperature and the long-term effect of upwelling, in that order, are the two major drivers.

Acknowledgements

Data for this study came from the Global Ocean Data Analysis Project Version 2 (GLODAPv2) and World Ocean Atlas 2013 version 2 (WOA13 V2). All the data used is publicly available at the Ocean Carbon Data System (OCADS, https://www.nodc.noaa.gov/ocads/oceans/GLODAPv2/) and National Oceanic and Atmospheric Administration (NOAA, and https://www.nodc.noaa.gov/OC5/woa13/woa13data.html). This study was funded by the Swire Educational Trust (PhD studentship to Yingxu Wu), and we also acknowledge funding by RAGNARoCC to M. P. Humphreys and T. Tyrrell (NE/K002546/1). We thank two anonymous reviewers for their careful reviews.

References

Assmy, P., Smetacek, V., Montresor, M., Klaas, C., Henjes, J., Strass, V. H., Arrieta, J. M., Bathmann, U., Berg, G. M., Breitbarth, E., Cisewski, B., Friedrichs, L., Fuchs, N., Herndl, G. J., Jansen, S., Krägefsky, S., Latasa, M., Peeken, I., Röttgers, R., Scharek, R., Schüller, S. E., Steigenberger, S., Webb, A., and Wolf-Gladrow, D.: Thick-shelled, grazer-protected diatoms decouple ocean carbon and silicon cycles in the iron-limited Antarctic Circumpolar Current, Proceedings of the National Academy of Sciences, 110, 20633-20638, http://doi.org/10.1073/pnas.1309345110, 2013.

Bakun, A.: Global climate change and intensification of coastal ocean upwelling, Science, 247, 198-201, http://doi.org/10.1126/science.247.4939.198, 1990.

Balch, W. M., Bates, N. R., Lam, P. J., Twining, B. S., Rosengard, S. Z., Bowler, B. C., Drapeau, D. T., Garley, R., Lubelczyk, L. C., Mitchell, C., and Rauschenberg, S.: Factors regulating the Great Calcite Belt in the Southern Ocean and its biogeochemical significance, Global Biogeochemical Cycles, 30, 1124-1144, http://doi.org/10.1002/2016GB005414, 2016.

Barton, E. D., Field, D. B., and Roy, C.: Canary current upwelling: More or less?, Progress in Oceanography, 116, 167-178, http://doi.org/10.1016/j.pocean.2013.07.007, 2013.

Bates, N., Astor, Y., Church, M., Currie, K., Dore, J., Gonaález-Dávila, M., Lorenzoni, L., Muller-Karger, F., Olafsson, J., and Santa-Casiano, M.: A time-series view of changing ocean chemistry due to ocean uptake of anthropogenic CO_2 and ocean acidification, Oceanography, 27, 126-141, 2014.

Bates, N. R., Pequignet, A. C., and Sabine, C. L.: Ocean carbon cycling in the Indian Ocean: 1. Spatiotemporal variability of inorganic carbon and air-sea CO_2 gas exchange, Global Biogeochemical Cycles, 20, GB3020, https://doi.org/10.1029/2005GB002491, 2006.

Boyer, T.P., Antonov, J. I., Baranova, O. K., Coleman, C., Garcia, H. E., Grodsky, A., Johnson, D. R., Locarnini, R. A., Mishonov, A. V., O'Brien, T. D., Paver, C. R., Reagan, J. R., Seidov, D., Smolyar, I. V. and Zweng, M. M.: World Ocean Database 2013, NOAA Atlas NESDIS 72, S. Levitus, Ed., A. Mishonov, Technical Ed.; Silver Spring, MD, pp. 209, http://doi.org/10.7289/V5NZ85MT, 2013.

5 Bozec, Y., Thomas, H., Schiettecatte, L. S., Borges, A. V., Elkalay, K., and de Baar, H. J. W.: Assessment of the processes controlling seasonal variations of dissolved inorganic carbon in the North Sea, Limnology and Oceanography, 51, 2746-2762, 2006.

Brewer, P. G., and Goldman, J. C.: Alkalinity changes generated by photoplankton growth, Limnology and Oceanography, 21, 108-117, 1976.

10 Broecker, W. S.: The salinity contrast between the Atlantic and Pacific oceans during glacial time, Paleoceanography, 4, 207-212, http://doi.org/10.1029/PA004i002p00207, 1989.

Cai, W. J., Hu, X., Huang, W. J., Jiang, L. Q., Wang, Y., Peng, T. H., and Zhang, X.: Alkalinity distribution in the western North Atlantic Ocean margins, Journal of Geophysical Research: Oceans, 115, C08014, https://doi.org/10.1029/2009JC005482, 2010.

15 Cameron, D. R., Lenton, T. M., Ridgwell, A. J., Shepherd, J. G., Marsh, R., and Yool, A.: A factorial analysis of the marine carbon cycle and ocean circulation controls on atmospheric CO_2, Global Biogeochemical Cycles, 19, GB4027, http://doi.org/10.1029/2005GB002489, 2005.

Capone, D. G., and Hutchins, D. A.: Microbial biogeochemistry of coastal upwelling regimes in a changing ocean, Nature Geoscience, 6, 711-717, http://doi.org/10.1038/ngeo1916, 2013.

20 Chavez, F. P., and Messié, M.: A comparison of eastern boundary upwelling ecosystems, Progress in Oceanography, 83, 80-96, http://doi.org/10.1016/j.pocean.2009.07.032, 2009.

Clargo, N. M., Salt, L. A., Thomas, H., and de Baar, H. J. W.: Rapid increase of observed DIC and pCO$_2$ in the surface waters of the North Sea in the 2001-2011 decade ascribed to climate change superimposed by biological processes, Marine Chemistry, 177, 566-581, http://doi.org/10.1016/j.marchem.2015.08.010, 2015.

25 de Boyer Montégut, C., Madec, G., Fischer, A. S., Lazar, A., and Iudicone, D.: Mixed layer depth over the global ocean: An examination of profile data and a profile-based climatology, Journal of Geophysical Research: Oceans, 109, C12003, http://doi.org/10.1029/2004JC002378, 2004.

Dickson, A. G., and Millero, F. J.: A comparison of the equilibrium constants for the dissociation of carbonic acid in seawater media, Deep Sea Research, 34, 1733-1743, 1987.

30 Dickson, A. G.: Standard potential of the reaction: AgCl (s)+ 12H$_2$ (g)= Ag (s)+ HCl (aq), and and the standard acidity constant of the ion HSO$_4^-$ in synthetic sea water from 273.15 to 318.15 K, The Journal of Chemical Thermodynamics, 22, 113-127, 1990.

Duarte, C. M., Regaudie-de-Gioux, A., Arrieta, J. M., Delgado-Huertas, A., and Agustí, S.: The oligotrophic ocean is heterotrophic, Annual Review of Marine Science, 5, 551-569, http://doi: 10.1146/annurev-marine-121211-172337, 2013.

Doney, S. C., Fabry, V. J., Feely, R. A., and Kleypas, J. A.: Ocean acidification: the other CO_2 problem, Annual review of marine science, 1, 169-192, http://doi.org/10.1146/annurev.marine.010908.163834, 2009.

Evans, W., Hales, B., Strutton, P. G., Shearman, R. K., and Barth, J. A.: Failure to bloom: Intense upwelling results in negligible phytoplankton response and prolonged CO_2 outgassing over the Oregon shelf, Journal of Geophysical Research: Oceans, 120, 1446-1461, http://doi.org/10.1002/2014JC010580, 2015.

Falkowski, P. G., Scholes, R. J., Boyle, E., Canadell, J., Canfield, D., Elser, J., Gruber, N., Hibbard, K., Högberg, P., Linder, S., Mackenzie, F. T., Moore III, B., Pedersen, T., Rosenthal, Y., Seitzinger, S., Smetacek, V., and Steffen, W.: The global carbon cycle: a test of our knowledge of Earth as a system, Science, 290, 291-296, http://doi.org/10.1126/science.290.5490.291, 2000.

Feely, R.A.: Ocean Acidification. In State of the Climate in 2007, Bulletin of the American Meteorological Society, 89, S58. https://doi.org/10.1175/1520-0477-89.7.S10, 2008.

Ferrari, R., Jansen, M. F., Adkins, J. F., Burke, A., Stewart, A. L., and Thompson, A. F.: Antarctic sea ice control on ocean circulation in present and glacial climates, Proceedings of the National Academy of Sciences, 111, 8753-8758, http://doi.org/10.1073/pnas.1323922111, 2014.

Friis, K., Körtzinger, A., and Wallace, D. W.: The salinity normalization of marine inorganic carbon chemistry data, Geophysical Research Letters, 30, 1080, http://doi.org/10.1029/2002GL015898, 2003.

Fornasini, P.: The uncertainty in physical measurements: an introduction to data analysis in the physics laboratory, Springer Science & Business Media, 2008.

Friis, K., Körtzinger, A., and Wallace, D. W.: The salinity normalization of marine inorganic carbon chemistry data, Geophysical Research Letters, 30, 1080, http://doi.org/10.1029/2002GL015898, 2003.

Fry, C. H., Tyrrell, T., Hain, M. P., Bates, N. R., and Achterberg, E. P.: Analysis of global surface ocean alkalinity to determine controlling processes, Marine Chemistry, 174, 46-57, http://doi.org/10.1016/j.marchem.2015.05.003, 2015.

Galbraith, E. D., and Martiny, A. C.: A simple nutrient-dependence mechanism for predicting the stoichiometry of marine ecosystems, Proceedings of the National Academy of Sciences, 112, 8199-8204, http://doi.org/10.1073/pnas.1423917112, 2015.

Gruber, N.: Anthropogenic CO_2 in the Atlantic Ocean, Global Biogeochemical Cycles, 12, 165-191, http://doi.org/10.1029/97GB03658, 1998.

Gruber, N., and Sarmiento, J. L.: Large-scale biogeochemical/physical interactions in elemental cycles, The Sea, 12, 337-399, 2002.

Holzer, M., Primeau, F. W., DeVries, T., and Matear, R.: The Southern Ocean silicon trap: Data-constrained estimates of regenerated silicic acid, trapping efficiencies, and global transport paths, Journal of Geophysical Research: Oceans, 119, 313-331, http://doi.org/10.1002/2013JC009356, 2014.

Humphreys, M. P., Griffiths, A. M., Achterberg, E. P., Holliday, N. P., Rérolle, V. M. C., Menzel Barraqueta, J.-L., Couldrey, M. P., Oliver, K. I. C., Hartman, S. E., Esposito, M., and Boyce, A. J.: Multidecadal accumulation of anthropogenic and

remineralized dissolved inorganic carbon along the Extended Ellett Line in the northeast Atlantic Ocean, Global Biogeochemical Cycles, 30, 293-310, http://doi.org/10.1002/2015GB005246, 2016.

Humphreys, M. P.: Climate sensitivity and the rate of ocean acidification: future impacts, and implications for experimental design, ICES Journal of Marine Science, 74, 934-940, http://doi.org/10.1093/icesjms/fsw189, 2017.

5   Humphreys, M. P., Daniels, C. J., Wolf-Gladrow, D. A., Tyrrell, T., and Achterberg, E. P.: On the influence of marine biogeochemical processes over CO_2 exchange between the atmosphere and ocean, Marine Chemistry, 199, 1-11, https://doi.org/10.1016/j.marchem.2017.12.006, 2018.

Jiang, L. Q., Feely, R. A., Carter, B. R., Greeley, D. J., Gledhill, D. K., and Arzayus, K. M.: Climatological distribution of aragonite saturation state in the global oceans, Global Biogeochemical Cycles, 29, http://doi.org/10.1002/2015GB005198,

10   2015.

Jiang, Z. P., Hydes, D. J., Tyrrell, T., Hartman, S. E., Hartman, M. C., Dumousseaud, C., Padin, X. A., Skjelvan, I., and González-Pola, C.: Key controls on the seasonal and interannual variations of the carbonate system and air-sea CO_2 flux in the Northeast Atlantic (Bay of Biscay), Journal of Geophysical Research: Oceans, 118, 785-800, http://doi.org/10.1002/jgrc.20087, 2013.

15   Jiang, Z. P., Tyrrell, T., Hydes, D. J., Dai, M., and Hartman, S. E.: Variability of alkalinity and the alkalinity-salinity relationship in the tropical and subtropical surface ocean, Global Biogeochemical Cycles, 28, 729-742, http://doi.org/10.1002/2013GB004678, 2014.

Key, R. M., Kozyr, A., Sabine, C. L., Lee, K., Wanninkhof, R., Bullister, J. L., Feely, R. A., Millero, F. J., Mordy, C., and Peng, T. H.: A global ocean carbon climatology: Results from Global Data Analysis Project (GLODAP), Global Biogeochemical

20   Cycles, 18, GB4031, http://doi.org/10.1029/2004GB002247, 2004.

Key, R. M., Olsen, A., van Heuven, S., Lauvset, S. K., Velo, A., Lin, X., Schirnick, C., Kozyr, A., Tanhua, T., and Hoppema, M.: Global Ocean Data Analysis Project, Version 2 (GLODAPv2), ORNL/CDIAC-162, NDP-093, http://doi.org/10.3334/CDIAC/OTG.NDP093_GLODAPv2, 2015.

Khatiwala, S., Tanhua, T., Mikaloff Fletcher, S., Gerber, M., Doney, S. C., Graven, H. D., Gruber, N., McKinley, G. A., Murata,

25   A., Ríos, A. F., and Sabine, C. L.: Global ocean storage of anthropogenic carbon, Biogeosciences, 10, 2169-2191, http://doi.org/10.5194/bg-10-2169-2013, 2013.

Landschützer, P., Gruber, N., Haumann, F. A., Rödenbeck, C., Bakker, D. C. E., van Heuven, S., Hoppema, M., Metzl, N., Sweeney, C., Takahashi, T., Tilbrook, B., and Wanninkhof, R.: The reinvigoration of the Southern Ocean carbon sink, Science, 349, 1221-1224, http://doi.org/10.1126/science.aab2620, 2015.

30   Lauvset, S. K., and Tanhua, T.: A toolbox for secondary quality control on ocean chemistry and hydrographic data, Limnology and Oceanography: Methods, 13, 601-608, http://doi.org/10.1002/lom3.10050, 2015.

Lauvset, S. K., Key, R. M., Olsen, A., van Heuven, S., Velo, A., Lin, X., Schirnick, C., Kozyr, A., Tanhua, T., Hoppema, M., Jutterström, S., Steinfeldt, R., Jeansson, E., Ishii, M., Perez, F. F., Suzuki, T., and Watelet, S.: A new global interior ocean mapped climatology: the 1° × 1° GLODAP version 2, Earth Syst. Sci. Data, 8, 325-340, http://doi.org/10.5194/essd-8-

325-2016, 2016.

Le Quéré, C., Andrew, R. M., Friedlingstein, P., Sitch, S., Pongratz, J., Manning, A. C., Korsbakken, J. I., Peters, G. P., Canadell, J. G., Jackson, R. B., Boden, T. A., Tans, P. P., Andrews, O. D., Arora, V. K., Bakker, D. C. E., Barbero, L., Becker, M., Betts, R. A., Bopp, L., Chevallier, F., Chini, L. P., Ciais, P., Cosca, C. E., Cross, J., Currie, K., Gasser, T., Harris, I., Hauck, J., Haverd, V., Houghton, R. A., Hunt, C. W., Hurtt, G., Ilyina, T., Jain, A. K., Kato, E., Kautz, M., Keeling, R. F., Klein Goldewijk, K., Körtzinger, A., Landschützer, P., Lefèvre, N., Lenton, A., Lienert, S., Lima, I., Lombardozzi, D., Metzl, N., Millero, F., Monteiro, P. M. S., Munro, D. R., Nabel, J. E. M. S., Nakaoka, S. I., Nojiri, Y., Padin, X. A., Peregon, A., Pfeil, B., Pierrot, D., Poulter, B., Rehder, G., Reimer, J., Rödenbeck, C., Schwinger, J., Séférian, R., Skjelvan, I., Stocker, B. D., Tian, H., Tilbrook, B., Tubiello, F. N., van der Laan-Luijkx, I. T., van der Werf, G. R., van Heuven, S., Viovy, N., Vuichard, N., Walker, A. P., Watson, A. J., Wiltshire, A. J., Zaehle, S., and Zhu, D.: Global Carbon Budget 2017, Earth Syst. Sci. Data, 10, 405-448, 10.5194/essd-10-405-2018, 2018.

Lee, K., Wanninkhof, R., Feely, R. A., Millero, F. J., and Peng, T. H.: Global relationships of total inorganic carbon with temperature and nitrate in surface seawater, Global Biogeochemical Cycles, 14, 979-994, http://doi.org/10.1029/1998gb001087, 2000.

Lee, K., Choi, S. D., Park, G. H., Wanninkhof, R., Peng, T. H., Key, R. M., Sabine, C. L., Feely, R. A., Bullister, J. L., Millero, F. J., and Kozyr, A.: An updated anthropogenic CO_2 inventory in the Atlantic Ocean, Global Biogeochemical Cycles, 17, 1116, http://doi.org/10.1029/2003GB002067, 2003.

Lee, K., Tong, L. T., Millero, F. J., Sabine, C. L., Dickson, A. G., Goyet, C., Park, G.-H., Wanninkhof, R., Feely, R. A., and Key, R. M.: Global relationships of total alkalinity with salinity and temperature in surface waters of the world's oceans, Geophysical Research Letters, 33, L19605, http://doi.org/10.1029/2006GL027207, 2006.

Lee, K., Kim, T.-W., Byrne, R. H., Millero, F. J., Feely, R. A., and Liu, Y.-M.: The universal ratio of boron to chlorinity for the North Pacific and North Atlantic oceans, Geochimica et Cosmochimica Acta, 74, 1801-1811, http://doi.org/10.1016/j.gca.2009.12.027, 2010.

Lueker, T. J., Dickson, A. G., and Keeling, C. D.: Ocean pCO_2 calculated from dissolved inorganic carbon, alkalinity, and equations for K1 and K2: validation based on laboratory measurements of CO_2 in gas and seawater at equilibrium, Marine Chemistry, 70, 105-119, http://doi.org/10.1016/S0304-4203(00)00022-0, 2000.

Lumpkin, R., and Speer, K.: Global ocean meridional overturning, Journal of Physical Oceanography, 37, 2550-2562, http://doi.org/10.1175/JPO3130.1, 2007.

Marinov, I., Gnanadesikan, A., Toggweiler, J. R., and Sarmiento, J. L.: The Southern Ocean biogeochemical divide, Nature, 441, 964-967, http://doi.org/10.1038/nature04883, 2006.

Marshall, J., and Speer, K.: Closure of the meridional overturning circulation through Southern Ocean upwelling, Nature Geoscience, 5, 171-180, 2012.

Martiny, A. C., Pham, C. T. A., Primeau, F. W., Vrugt, J. A., Moore, J. K., Levin, S. A., and Lomas, M. W.: Strong latitudinal patterns in the elemental ratios of marine plankton and organic matter, Nature Geoscience, 6, 279-283,

http://doi.org/10.1038/ngeo1757, 2013.

McGregor, H. V., Dima, M., Fischer, H. W., and Mulitza, S.: Rapid 20th-Century Increase in Coastal Upwelling off Northwest Africa, Science, 315, 637-639, http://doi.org/10.1126/science.1134839, 2007.

Merlivat, L., Boutin, J., and Antoine, D.: Roles of biological and physical processes in driving seasonal air–sea CO_2 flux in the Southern Ocean: New insights from CARIOCA pCO_2, Journal of Marine Systems, 147, 9-20, http://doi.org/10.1016/j.jmarsys.2014.04.015, 2015.

Mikaloff-Fletcher, S. E.: An increasing carbon sink?, Science, 349, 1165, http://doi.org/10.1126/science.aad0912, 2015.

Millero, F. J., Degler, E. A., O'Sullivan, D. W., Goyet, C., and Eischeid, G.: The carbon dioxide system in the Arabian Sea, Deep Sea Research Part II: Topical Studies in Oceanography, 45, 2225-2252, http://doi.org/10.1016/S0967-0645(98)00069-1, 1998.

Moore, C. M., Mills, M. M., Arrigo, K. R., Berman-Frank, I., Bopp, L., Boyd, P. W., Galbraith, E. D., Geider, R. J., Guieu, C., Jaccard, S. L., Jickells, T. D., La Roche, J., Lenton, T. M., Mahowald, N. M., Maranon, E., Marinov, I., Moore, J. K., Nakatsuka, T., Oschlies, A., Saito, M. A., Thingstad, T. F., Tsuda, A., and Ulloa, O.: Processes and patterns of oceanic nutrient limitation, Nature Geoscience, 6, 701-710, http://doi.org/10.1038/ngeo1765, 2013.

Moore, C. M.: Diagnosing oceanic nutrient deficiency, Philosophical Transactions of the Royal Society A, 374, 20152090, http://doi.org/10.1098/rsta.2015.0290, 2016.

Morrison, A. K., Frölicher, T. L., and Sarmiento, J. L.: Upwelling in the Southern Ocean, Physics Today, 68, 27-32, http://doi.org/10.1063/pt.3.2654, 2015.

Murray, J. W., Barber, R. T., Roman, M. R., Bacon, M. P., and Feely, R. A.: Physical and biological controls on carbon cycling in the Equatorial Pacific, Science, 266, 58-65, http://doi.org/10.1126/science.266.5182.58, 1994.

Nielsdóttir, M. C., Moore, C. M., Sanders, R., Hinz, D. J., and Achterberg, E. P.: Iron limitation of the postbloom phytoplankton communities in the Iceland Basin, Global Biogeochemical Cycles, 23, GB3001, http://doi.org/10.1029/2008GB003410, 2009.

Olsen, A., Key, R. M., van Heuven, S., Lauvset, S. K., Velo, A., Lin, X., Schirnick, C., Kozyr, A., Tanhua, T., Hoppema, M., Jutterström, S., Steinfeldt, R., Jeansson, E., Ishii, M., Pérez, F. F., and Suzuki, T.: The Global Ocean Data Analysis Project version 2 (GLODAPv2) – an internally consistent data product for the world ocean, Earth Syst. Sci. Data, 8, 297-323, http://doi.org/10.5194/essd-8-297-2016, 2016.

Omta, A. W., Dutkiewicz, S., and Follows, M. J.: Dependence of the ocean-atmosphere partitioning of carbon on temperature and alkalinity, Global Biogeochemical Cycles, 25, GB1003, https://doi: 10.1029/2010GB003839, 2011.

Orr, J. C., Fabry, V. J., Aumont, O., Bopp, L., Doney, S. C., Feely, R. A., Gnanadesikan, A., Gruber, N., Ishida, A., Joos, F., Key, R. M., Lindsay, K., Maier-Reimer, E., Matear, R., Monfray, P., Mouchet, A., Najjar, R. G., Plattner, G.-K., Rodgers, K. B., Sabine, C. L., Sarmiento, J. L., Schlitzer, R., Slater, R. D., Totterdell, I. J., Weirig, M.-F., Yamanaka, Y., and Yool, A.: Anthropogenic ocean acidification over the twenty-first century and its impact on calcifying organisms, Nature, 437, 681-686, http://doi.org/10.1038/nature04095, 2005.

Postma, H.: The exchange of oxygen and carbon dioxide between the ocean and the atmosphere, Netherlands Journal of Sea Research, 2, 258-283, http://doi.org/10.1016/0077-7579(64)90013-4, 1964.

Redfield, A. C.: The influence of organisms on the composition of sea-water, The Sea, 26-77, 1963.

Ruttenberg, K. C.: The Global Phosphorus Cycle, in: Treatise on Geochemistry, edited by: Turekian, K. K., Pergamon, Oxford, 585-643, 2003.

Sabine, C. L., Key, R. M., Johnson, K. M., Millero, F. J., Poisson, A., Sarmiento, J. L., Wallace, D. W. R., and Winn, C. D.: Anthropogenic CO_2 inventory of the Indian Ocean, Global Biogeochemical Cycles, 13, 179-198, http://doi.org/10.1029/1998GB900022, 1999.

Sabine, C. L., Key, R. M., Feely, R. A., and Greeley, D.: Inorganic carbon in the Indian Ocean: Distribution and dissolution processes, Global Biogeochemical Cycles, 16, 1067, http://doi.org/10.1029/2002GB001869, 2002.

Sarmiento, J. L., Gruber, N., Brzezinski, M. A., and Dunne, J. P.: High-latitude controls of thermocline nutrients and low latitude biological productivity, Nature, 427, 56-60, http://doi.org/10.1038/nature02127, 2004a.

Sarmiento, J. L., Slater, R., Barber, R., Bopp, L., Doney, S. C., Hirst, A. C., Kleypas, J., Matear, R., Mikolajewicz, U., Monfray, P., Soldatov, V., Spall, S. A., and Stouffer, R.: Response of ocean ecosystems to climate warming, Global Biogeochemical Cycles, 18, GB3003, http://doi.org/10.1029/2003GB002134, 2004b.

Sarmiento, J. L., and Gruber, N.: Ocean Biogeochemical Dynamics, Princeton University Press, 582 pp., 2006.

Sasse, T. P., McNeil, B. I., and Abramowitz, G.: A novel method for diagnosing seasonal to inter-annual surface ocean carbon dynamics from bottle data using neural networks, Biogeosciences, 10, 4319-4340, http://doi.org/10.5194/bg-10-4319-2013, 2013.

Takahashi, T., Sutherland, S. C., Wanninkhof, R., Sweeney, C., Feely, R. A., Chipman, D. W., Hales, B., Friederich, G., Chavez, F., and Sabine, C.: Climatological mean and decadal change in surface ocean $p$$CO_2$, and net sea–air CO_2 flux over the global oceans, Deep Sea Research II, 56, 554-577, 2009.

Takahashi, T., Sutherland, S. C., Chipman, D. W., Goddard, J. G., Ho, C., Newberger, T., Sweeney, C., and Munro, D. R.: Climatological distributions of pH, $p$$CO_2$, total CO_2, alkalinity, and $CaCO_3$ saturation in the global surface ocean, and temporal changes at selected locations, Marine Chemistry, 164, 95-125, http://doi.org/10.1016/j.marchem.2014.06.004, 2014.

Talley, L. D.: Closure of the global overturning circulation through the Indian, Pacific, and Southern Oceans: Schematics and transports, Oceanography, 26, 80-97, http://doi.org/10.5670/oceanog.2013.07, 2013.

Toggweiler, J. R., Gnanadesikan, A., Carson, S., Murnane, R., and Sarmiento, J. L.: Representation of the carbon cycle in box models and GCMs: 1. Solubility pump, Global Biogeochemical Cycles, 17, 1026, http://doi.org/10.1029/2001GB001401, 2003a.

Toggweiler, J. R., Murnane, R., Carson, S., Gnanadesikan, A., and Sarmiento, J. L.: Representation of the carbon cycle in box models and GCMs, 2, Organic pump, Global Biogeochemical Cycles, 17, 1027, http://doi.org/10.1029/2001GB001841, 2003b.

Tyrrell, T.: The relative influences of nitrogen and phosphorus on oceanic primary production, Nature, 400, 525-531, http://doi.org/10.1038/22941, 1999.

van Heuven, S., Pierrot, D., Rae, J.W.B., Lewis, E. and Wallace, D.W.R.: MATLAB Program Developed for CO_2 System Calculations, ORNL/CDIAC-105b, Carbon Dioxide Information Analysis Center, Oak Ridge National Laboratory, U.S.

5 Department of Energy, Oak Ridge, Tennessee, https://doi.org/10.3334/CDIAC/otg.CO2SYS_MATLAB_v1.1, 2011.

Vance, D., Little, S. H., de Souza, G. F., Khatiwala, S., Lohan, M. C., and Middag, R.: Silicon and zinc biogeochemical cycles coupled through the Southern Ocean, Nature Geoscience, 10, 202-206, http://doi.org/10.1038/ngeo2890, 2017.

Vázquez-Rodríguez, M., Touratier, F., Lo Monaco, C., Waugh, D. W., Padin, X. A., Bellerby, R. G. J., Goyet, C., Metzl, N., Ríos, A. F., and Pérez, F. F.: Anthropogenic carbon distributions in the Atlantic Ocean: data-based estimates from the

10 Arctic to the Antarctic, Biogeosciences, 6, 439-451, http://doi.org/10.5194/bg-6-439-2009, 2009.

Wang, D., Gouhier, T. C., Menge, B. A., and Ganguly, A. R.: Intensification and spatial homogenization of coastal upwelling under climate change, Nature, 518, 390-394, http://doi.org/10.1038/nature14235, 2015.

Weiss, R. F.: Carbon dioxide in water and seawater: the solubility of a non-ideal gas, Marine chemistry, 2, 203-215, 1974.

Williams, R. G., and Follows, M. J.: Ocean dynamics and the carbon cycle: Principles and mechanisms, Cambridge University

15 Press, 404 pp., 2011.

Wolf-Gladrow, D. A., Zeebe, R. E., Klaas, C., Kortzinger, A., and Dickson, A. G.: Total alkalinity: The explicit conservative expression and its application to biogeochemical processes, Marine Chemistry, 106 (1-2), 287-300, http://doi.org/10.1016/j.marchem.2007.01.006, 2007.

Yasunaka, S., Nojiri, Y., Nakaoka, S.-i., Ono, T., Mukai, H., and Usui, N.: Monthly maps of sea surface dissolved inorganic

20 carbon in the North Pacific: Basin-wide distribution and seasonal variation, Journal of Geophysical Research: Oceans, 118, 3843-3850, http://doi.org/10.1002/jgrc.20279, 2013.

Zeebe, R. E., and Wolf-Gladrow, D. A.: CO_2 in seawater: equilibrium, kinetics, isotopes, Elsevier Oceanography Series, 346 pp., 2001.

Table 1.

Definitions of Subscripts and Main Terms used in the Text. X represents any variable involved in the calculations. The program CO_2SYS was used to calculate values under different conditions.

Subscript	Meaning
Referring to (n)DIC values at a particular location	
X_{supply}	Value at depth, along isopycnals that upwell at this location
X_{surf}	Predicted value in the surface layer
X_{obs}	Observed value at this surface location
Referring to predicted (n)DIC values under different conditions	
$X_{SST=27}$	Predicted value with sea surface temperature changed to 27°C
X_{nonupw}	Predicted value with upwelled TA subtracted
Referring to changes in (n)DIC values because of processes	
ΔX_{Fe}	Effect of iron limitation (biological drawdown that is prevented)
ΔX_{temp}	Effect of sea surface temperature variations
ΔX_{upw_st}	Short-term effect of upwelling, through upwelled DIC
ΔX_{upw_lt}	Long-term effect of upwelling, through upwelled TA
Carbonate variables used to calculate predicted DIC values with CO_2SYS	
$DIC_{SST=27} = f\,(T_{SST=27}, S_{in\text{-}situ}, TA_{in\text{-}situ}, pCO_{2,in\text{-}situ})$	$DIC_{SST=27}$ is a function of in-situ S, TA, and pCO_2, and SST at 27°C
$DIC_{nonupw} = f\,(T_{in\text{-}situ}, S_{in\text{-}situ}, TA_{nonupw}, pCO_{2,in\text{-}situ})$	DIC_{nonupw} is a function of in-situ SST, S, and pCO_2, and pre-upwelling TA

Table 2.

Uncertainties for variables in this study.

Initial Variable	Uncertainty	Reference
Salinity	0.005	Olsen et al. (2016)
Phosphate	0.05 µmol kg^{-1}	Olsen et al. (2016)
DIC	4 µmol kg^{-1}	Olsen et al. (2016)
TA	6 µmol kg^{-1}	Olsen et al. (2016)
pCO$_2$	6.8 µatm	Takahashi et al. (2014)
DIC normalized to 2005	5.0 µmol kg^{-1}	derived in this study[a]
Alk*	6.1 µmol kg^{-1}	Modified from Fry et al. (2015)
nPhos$_{supply}$, Alk$^*_{supply}$, nDIC$_{supply}$	See text in Sect. 2.4.3	derived in this study[b]
Calculated Propagated Uncertainties		
ΔnDIC$_{temp}$	8.0 µmol kg^{-1}	derived in this study
ΔnDIC$_{upw\_st}$	5.4 µmol kg^{-1}	derived in this study
ΔnDIC$_{upw\_lt}$	8.9 µmol kg^{-1}	derived in this study

[a]the uncertainty of DIC normalized to 2005 was primarily propagated from TA and pCO$_{2,sw}^{2005}$. The uncertainty of pCO$_{2,sw}^{2005}$ was calculated from error propagation (Fornasini, 2008), to be 0.17 µatm.

5   [b]the uncertainties for variables with subscript "supply" were from their standard error of the mean.

Table 3.

Global and Regional Correlations Between DIC, nDIC and SST, Latitude.

Ocean	Region	DIC vs. Lat ρ[a]	DIC vs. Lat N[b]	nDIC vs. Lat ρ	nDIC vs. Lat N	DIC vs. SST ρ	DIC vs. SST N	nDIC vs. SST ρ	nDIC vs. SST N
Global		**0.71**	14228	**0.86**	14228	**-0.78**	14228	**-0.94**	14228
Southern Ocean	S of 40° S	**0.79**	3061	**0.81**	3061	**-0.93**	3061	**-0.95**	3061
North Atlantic	N of 40° N	**0.30**	1640	**0.58**	1640	**-0.34**	1640	**-0.78**	1640
North Pacific	N of 40° N	**0.02**	1601	**0.34**	1601	**-0.78**	1601	**-0.87**	1601

[a]the Spearman's rank correlation coefficient, for assessing monotonic relationships (there is a non-linear relationship between SST and CO_2 solubility). Statistically significant correlations are shown in bold.

5   [b]The number of data points from that area that were used in calculating the correlations.

Table 4.

Summary of nDIC Differences Between Low and High Latitudes. Each ΔnDIC value is the amount by which the average nDIC value for the high latitude region exceeds the average value for the low latitudes (30° S to 30° N). %'s in brackets represent the ratio to the observed nDIC difference in column 2. n.c. = not calculated.

Region[a]	Observed ΔnDIC ($\mu mol\ kg^{-1}$)	$\Delta nDIC_{temp}$ ($\mu mol\ kg^{-1}$)	$\Delta nDIC_{upw\_st}$ ($\mu mol\ kg^{-1}$)	$\Delta nDIC_{upw\_lt}$ ($\mu mol\ kg^{-1}$)
Southern Ocean	223	182 (82%)	220 (98%)	74 (33%)
North Atlantic	114	122 (107%)	n.c.	n.c.
North Pacific	192	137 (71%)	n.c.	n.c.

5   [a]The regions are defined as follows: North Atlantic: 40° N - 60° N; North Pacific: 40° N - 60° N; Southern Ocean: S of 40° S.
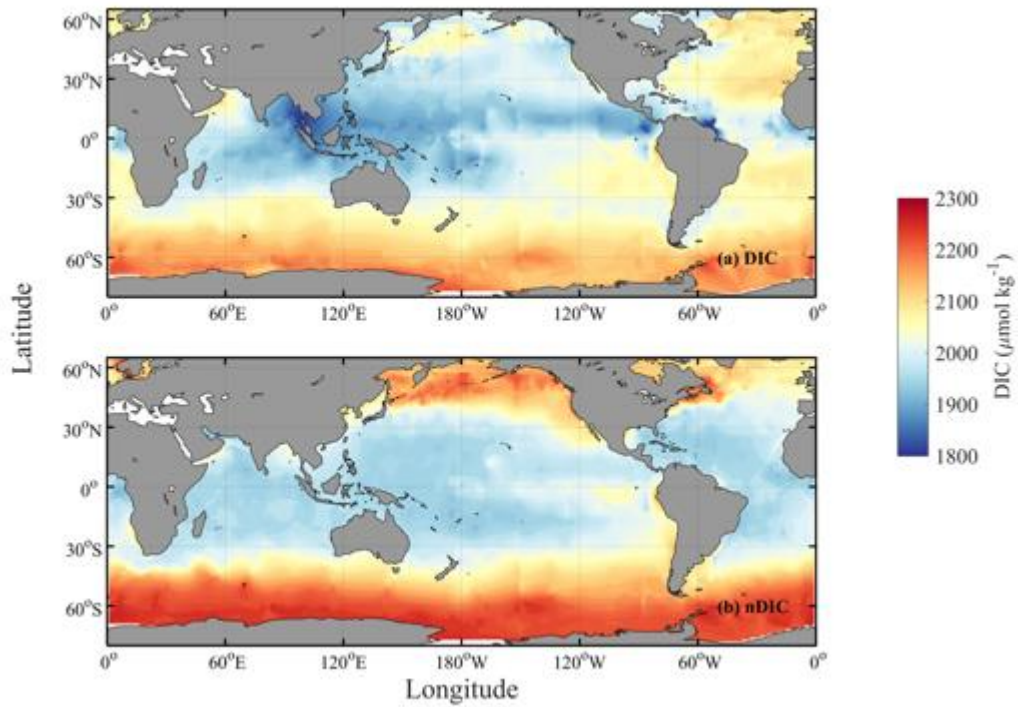
Figure 1. Spatial distributions of DIC and nDIC. (a) DIC (normalized to year 2005), (b) salinity-normalized DIC (nDIC, DIC normalized to reference year of 2005 and salinity of 35) in the surface global ocean. The latitudinal trends are clear, particularly for nDIC.
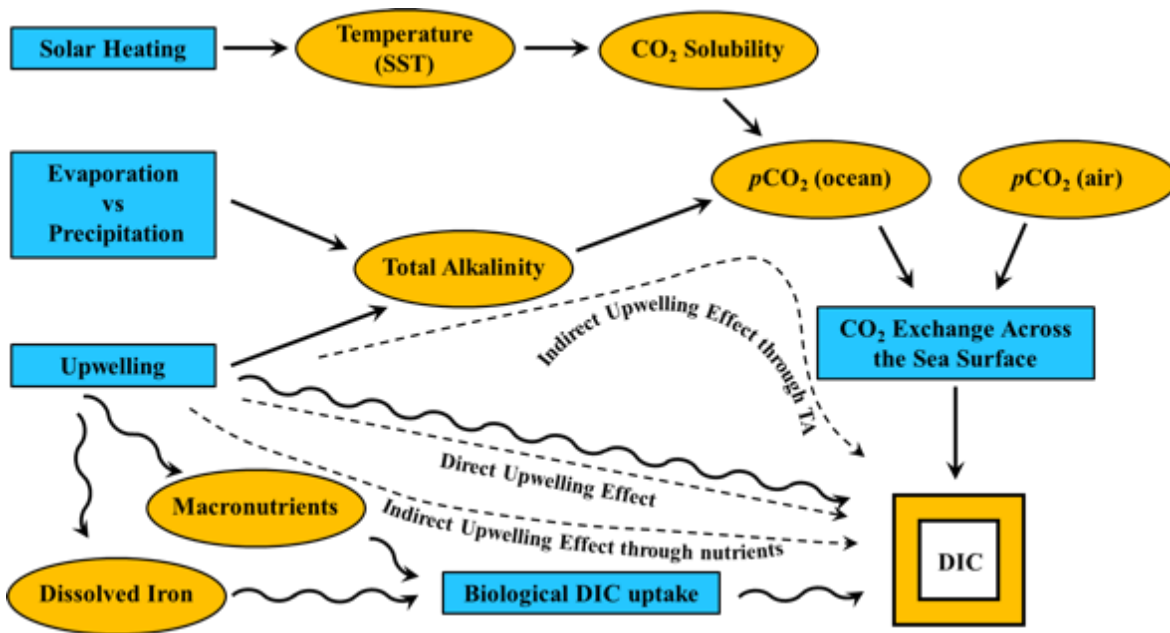
Figure 2. Major controls on surface DIC. Schematic showing the main processes exerting an influence over the concentration of DIC in the global surface ocean (producing variation with latitude). Blue shapes are processes and orange shapes are variables. Straight solid arrows represent equilibrium processes regulating nDIC in the long-term and wavy solid arrows represent disequilibrium processes regulating nDIC in the short-term. In the manuscript, we evaluate the upwelling effect on surface DIC in the Southern Ocean. Dashed arrows with text denote the three different ways that upwelling affects DIC: the direct effect through upwelled DIC; the indirect effect through upwelled nutrients which stimulates biological removal of DIC; and the indirect effect through upwelled TA in changing the equilibrium DIC with the atmosphere.
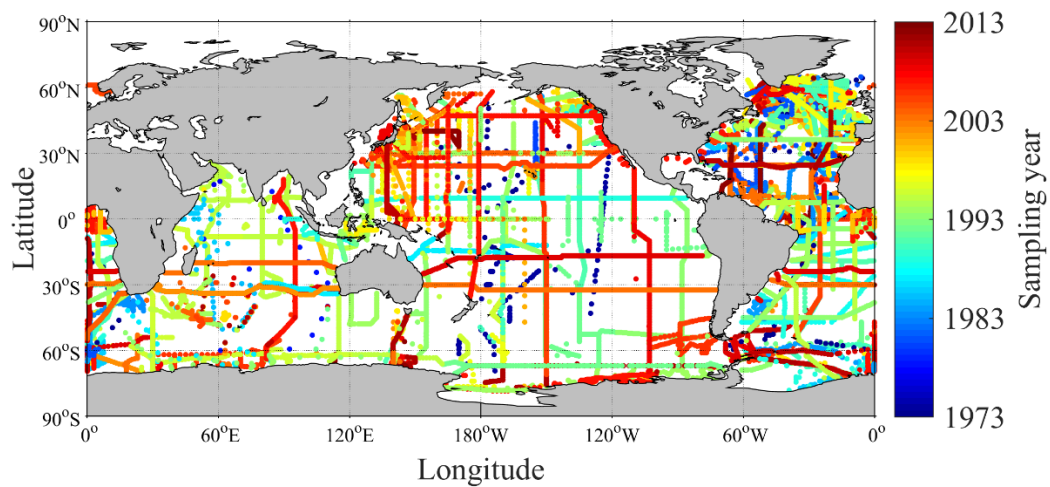
Figure 3. Spatial and temporal distribution of GLODAPv2 sampling stations used for this study.
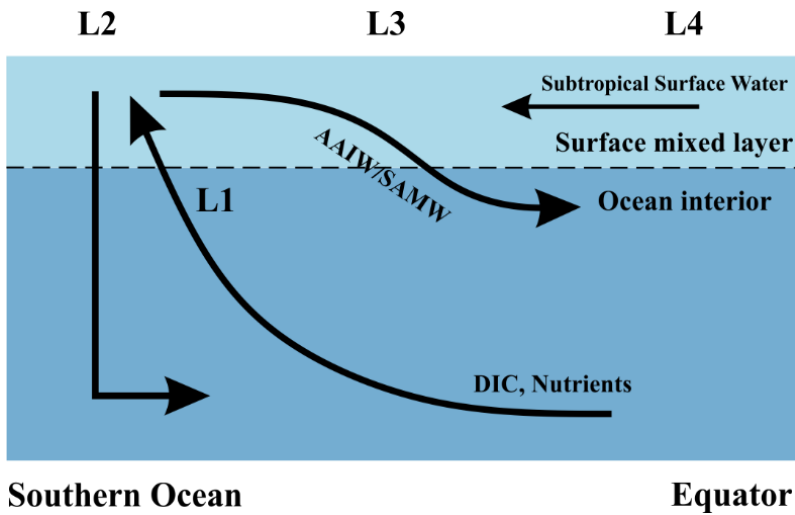
Figure 4. A schematic illustrating locations of interest and assumed major flow paths in the Southern Ocean. Black arrows represent the flow directions of water masses. The lower curved arrow denotes upwelling of deep water along isopycnal surfaces, and the upper curved arrow denotes subduction to form Subantarctic Mode Water (SAMW) and Antarctic Intermediate Water (AAIW). L1: upwelling water below the mixed layer, prior to any influence of surface processes; L2: sea surface within the core of the Southern Ocean upwelling south of 50° S (Morrison et al., 2015); L3: sea surface from 30° S to 50° S; L4: sea surface north of 30° S which experiences no direct effects from upwelling in the Southern Ocean.
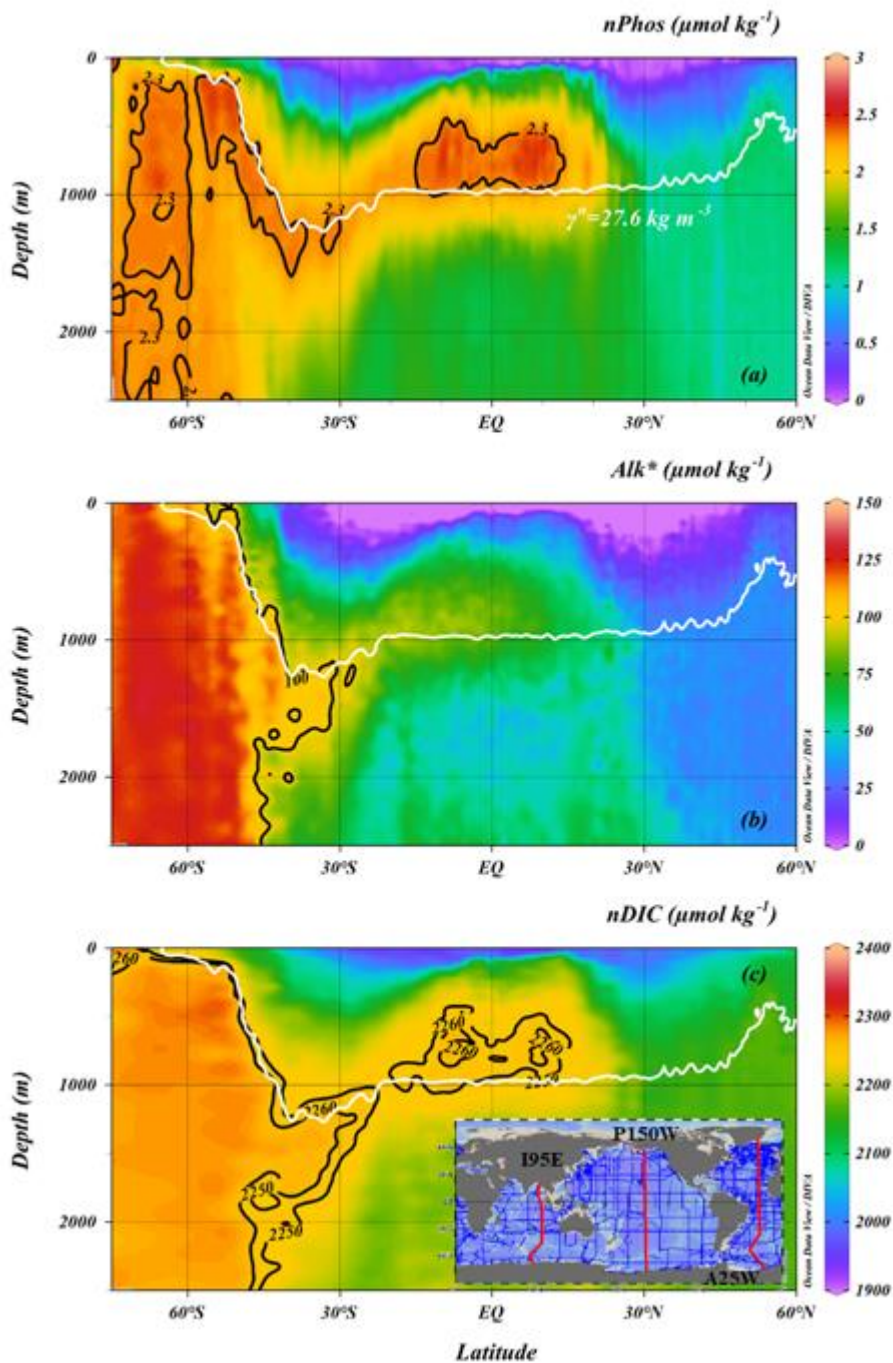
Figure 5. Vertical distributions of (a) nPhos, (b) Alk* and (c) nDIC along the Atlantic Ocean section. The Indian and Pacific sections are not shown. The selected Atlantic section (A25W) is shown as the red line on the right-hand side of the inset. The neutral density isopycnal along which upwelling occurs is indicated by the white contour, with the black contours referring to the observed variable.
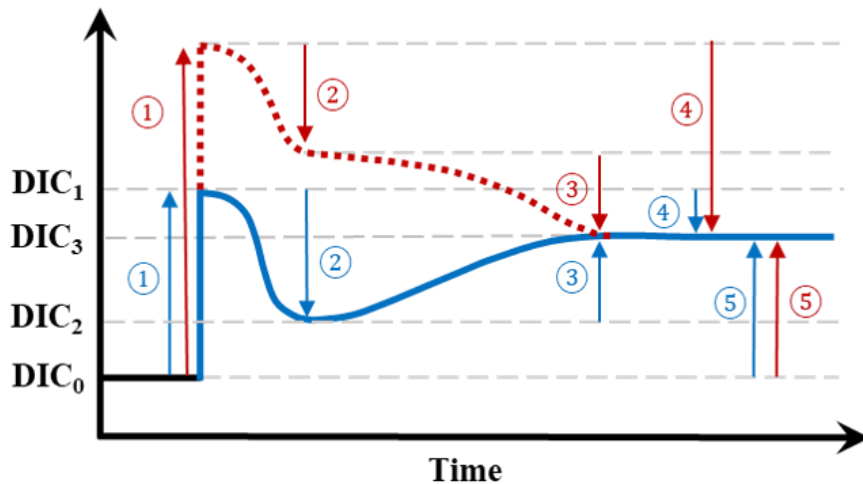
Figure 6. A schematic illustrating the various effects of upwelling on surface DIC. Numbers represent processes changing surface DIC, arrows point in the direction of change: ①: the *direct effect* of upwelling which elevates surface DIC from DIC_0 to DIC_1; ②: the DIC uptake by biology supported by upwelled nutrients, dropping DIC from DIC_1 to DIC_2. The processes of ① and ② make up the *short-term* effect of upwelling (i.e., difference between DIC_2 and DIC_0); ③: the change brought about by air-sea CO_2 gas exchange which continues towards the equilibrium with the atmosphere (DIC_3, whose level is determined by the amount of upwelled TA as well as by temperature); ④: the combination of both ② and ③ makes up the total *indirect effect* of upwelling (the difference between DIC_3 and DIC_1); ⑤: the *long-term* impact of upwelling on the level of surface DIC is the difference between DIC_3 and DIC_0. Blue and red indicate two scenarios with different amounts of upwelled DIC relative to upwelled TA, but the same amounts of upwelled TA. Blue is for upwelled water with a deficit in additional DIC relative to additional TA whereas red is for an excess in DIC relative to TA.
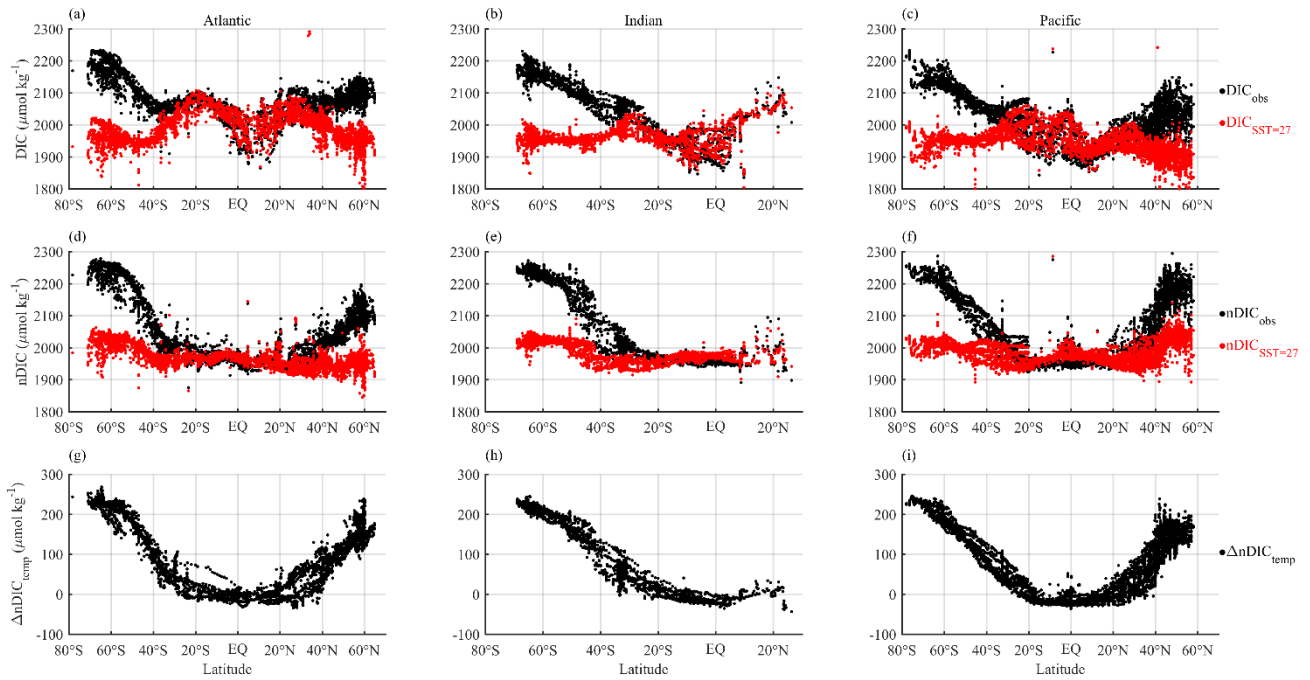
Figure 7. Latitudinal distributions of calculated temperature effect on surface DIC. Different columns show different basins (Atlantic, Indian and Pacific) and different rows show different calculated DIC variables. a, b and c show the observed surface DIC (black) and predicted DIC at SST of 27°C (red). d, e and f show the observed surface nDIC (black) and predicted nDIC at SST of 27°C (red). g, h and i show $\Delta nDIC_{temp}$, where $nDIC_{SST=27}$ is subtracted from $nDIC_{obs}$ to obtain the calculated temperature effect.
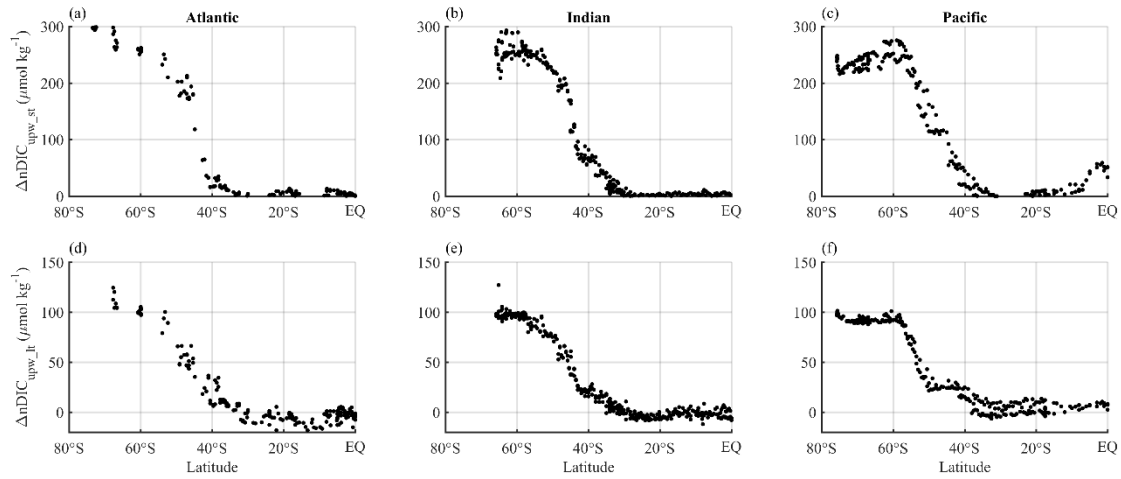
Figure 8. Latitudinal distributions of calculated upwelling effects on surface nDIC. Different columns show different sectors in ocean basins (Atlantic, Indian and Pacific) and different rows show different calculated effects on surface DIC. a, b and c show the short-term effect of upwelling ($\Delta nDIC_{upw\_st}$), which is driven by the direct supply of DIC from deep water and subsequent change by biology in the Southern Ocean. d, e and f show the long-term effect of upwelling ($\Delta nDIC_{upw\_lt}$), which is the difference between the observed nDIC value (determined mainly by the amount of upwelled TA, as well as by SST) and pre-upwelling nDIC value.
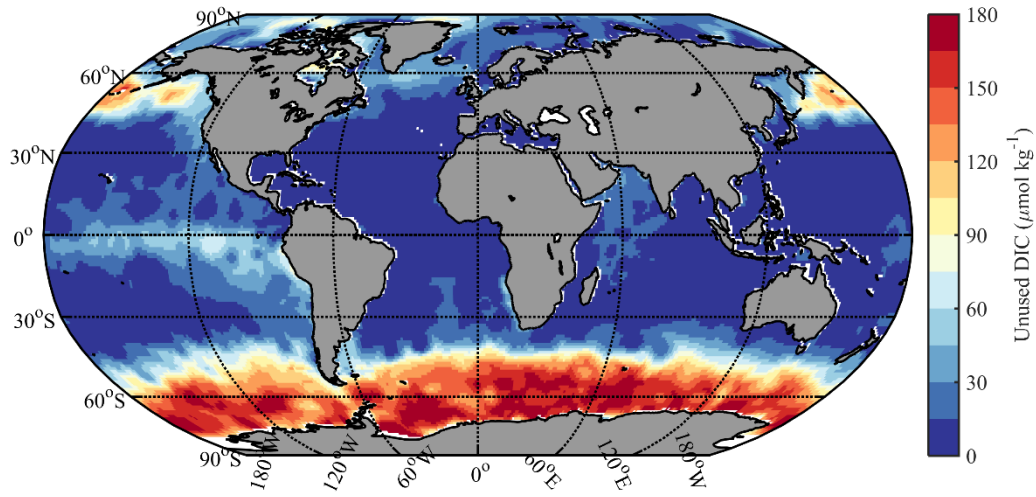
Figure 9. Calculated potential impact of iron limitation on surface DIC. Different colors correspond to different amounts of "unused DIC", calculated by Redfield ratio from observed residual phosphate.
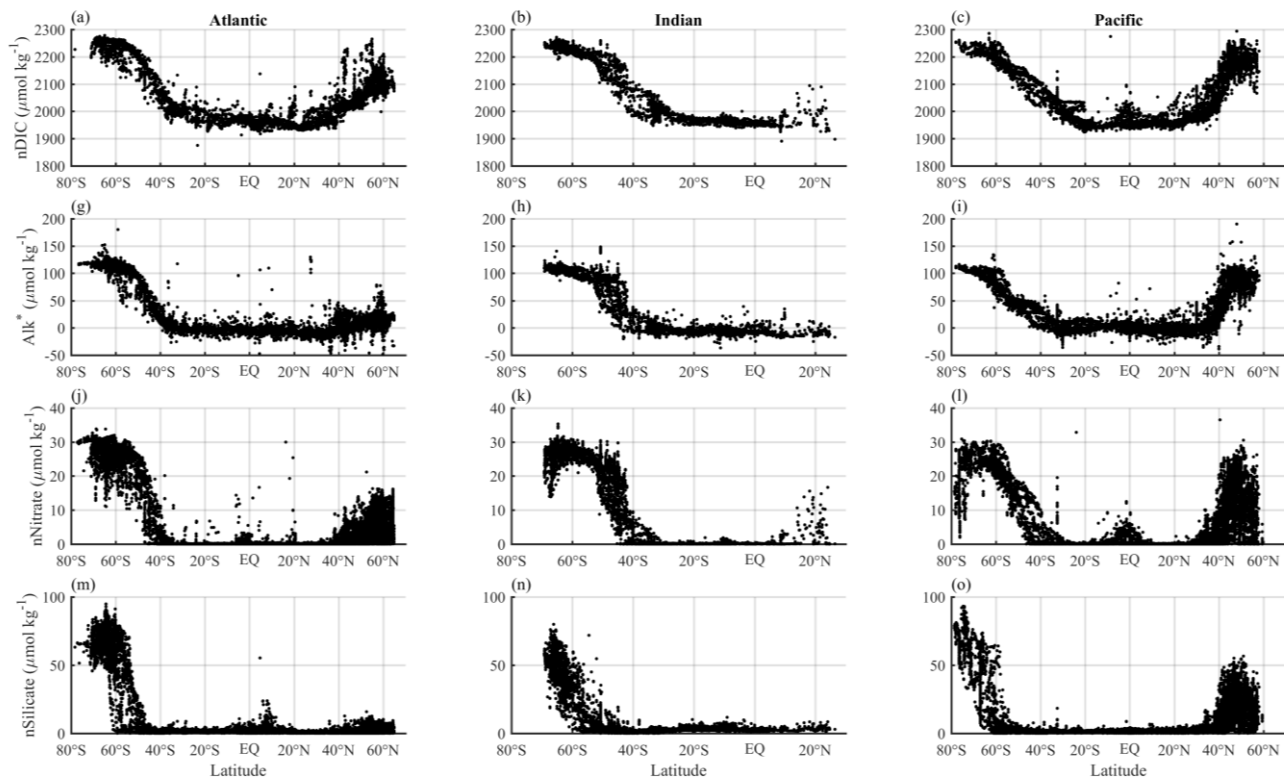
Figure 10. Latitudinal distributions of sea surface nDIC, Alk* (*Fry et al.*, 2015), salinity-normalized nitrate and silicate in each ocean basin.